

Theory of Quantum Interference in Molecular Junctions

Afaf Alqorashi

PhD Thesis in Physics

Submitted in part fulfilment of the requirements for
the degree of Doctor of Philosophy

January 10, 2018



Declaration

Except where stated otherwise, this thesis is a result of the author's original work and has not been submitted in whole or in part for the award of a higher degree elsewhere. This thesis documents work carried out between October 2014 and January 2018 at Lancaster University, UK, under the supervision of Prof. Colin J. Lambert and funded by Taif University, Saudi Arabia.

Afaf Alqorashi
January 10th, 2018

*To my beloved parents and husband
for their love, endless support,
encouragement and sacrifices.*

Abstract

In recent years, electron transport through single molecules has attracted huge attention, since the molecules are promising building blocks for the next generation of electronic devices. To create molecular junctions and probe their electrical properties, intense experimental efforts and theoretical studies are underway. For single molecule electronic applications, an important property is their electrical conductance. In this context, I start my thesis by introducing a general discussion about some basic topics related to single molecule transport theory.

Quantum interference effects have recently attracted great interest in studies of the charge transport at the single molecule scale. Within this framework, I study the single molecule conductances of five-membered ring compounds to investigate the effect of molecular symmetry and quantum interference on the charge transport through single molecule junctions. This theoretical and experimental study highlights the presence of destructive quantum interference and more importantly reveals that the control of molecular asymmetry via the heteroatom substitution allows the tuning of destructive quantum interference. Theoretically, I identify similar features over some

range of energies using different anchoring groups and elucidate the impact of the anchoring groups on the charge transport through single molecule. Moreover, I find that molecular symmetry has a slight effect on the binding energies of the **1-8** compounds seen in Figure 3.1.

Within the phase coherent regime, electron transport through a single molecule junction is described by the transmission coefficient, which describes how electrons pass through a molecule from one electrode to the other. Predicting features related to the transmission coefficient is a powerful tool for probing the electronic structure of molecular systems. In this connection, mid-gap transport theory is considered an efficient and easy method, which utilizes a magic ratio rule (MRR) to predict electrical conductance ratios associated with constructive quantum interference in aromatic molecules. I demonstrate that the MRR can be also applied for antiaromatic molecules and provide a comparison between the transmission coefficients of the aromatic and antiaromatic molecules. Furthermore, I present a theoretical study to investigate the transport properties of C_{60} using carbon-carbon triple bond anchoring groups and prove the validity of MRR when applied to such non-aromatic molecule.

Acknowledgements

First and foremost, I would like to thank ALLAH for giving me the strength, knowledge and ability to achieve my dream. During the completion of this thesis, there were many kinds of supports I have got. I would like to express my sincere gratitude to my supervisor, Professor Colin J. Lambert, whose selfless time and care were sometimes all that kept me going, for the continuous support of my Ph.D study, for his patience, motivation, and immense knowledge. His guidance helped me in all the time of research and writing of my thesis. I could not have imagined having a better supervisor for my Ph.D study.

Also I would like to thank my co- supervisor, Dr. Sara Sangtarash, for her excellent guidance, caring, patience, answering questions and providing me with many useful suggestions. Her academic and emotional support pushes me to carry on and follow my dream.

My sincere thanks also go to Dr. Hatef Sadeghi, Dr. Steven Bailey and Dr. Iain Grace for helping me to use the SIESTA DFT and GULLOM codes. I also would like to thank my external collaborators Prof. Wenjing Hong

(Xiamen University, China) and Prof. Martin Bryce (Durham University) and their groups for their efforts in the synthesis and measurements.

I also would like to extend my gratitude to my Ph.D colleagues; Qusiy, Eman, Mohammed, Mrjan, Alaa, Mohsin, Ali, Zain, and Qinqqing for their kind help and support. I also want to thank all my colleagues in physics department.

I want to thank my sponsor, the Ministry of Higher Education in Saudi Arabia, Saudi culture mission in London and Taif University in Saudi Arabia, for given me this opportunity to study a Ph.D. in the United Kingdom.

I would like to express a deep sense of gratitude to my beloved parents, words are insufficient to express all my gratitude to them for their endless love, care, support, encouragement and understanding. Also, I would like to give very special thanks to my beloved husband, thank you very much for your patience, tolerance, care and love for me. I could never have reached this stage without your support. I am also grateful to my children for being very cooperative and helpful. My gratitude to them is beyond words.

Last but not the least, my warm thanks also go to my sister, my brothers and the other family members for supporting me spiritually and virtually to follow my dream of getting this degree.

List of publication

1. Yang Yang; Markus Gantenbein; Afaf Alqorashi; Junying Wei; Sara Sangtarash; Duan Hu; Hatef Sadeghi; Rui Zhang; Jiuchan Pi; Ruihao Li; Junyang Liu; Jia Shi; Wenjing Hong; Colin J Lambert; Martin R Bryce. *Heteroatom-Induced Molecular Asymmetry Tunes Quantum Interference in Charge Transport through Single-Molecule Junctions.*
(Submitted).

Contents

1	Molecular Electronics.....	10
1.1	Introduction	10
1.2	Thesis Outline.....	23
2	Single Molecule Transport Theory	29
2.1	Introduction	29
2.2	Schrodinger Equation	30
2.3	The Landuaer Formula	32
2.4	Landauer-Buttiker Formalism	36
2.5	Green's Functions.....	37
2.5.1	Green's Function of Doubly Infinite Chain	38
2.5.2	Green's Function of Semi-Infinite One-Dimensional Chain	40
2.5.3	Green's Function of a Finite One-Dimensional Chain	42
2.5.4	One Dimensional Scattering.....	43
2.6	Transport Through an Arbitrary Scattering Region	45
2.7	Features of the Transport Curve	49
2.7.1	Breit-Wigner Resonance	49
2.7.2	Fano Resonances	51
2.7.3	Anti-Resonance	52
2.8	Magic Ratio Rule.....	53
2.9	M-theory:	57

2.10	Calculating binding energy using the counter poise method.....	61
3	Heteroatom Induced Molecular Asymmetry Tunes Quantum Interference in Charge Transport through Single-molecule Junctions with Five-membered Rings.	67
3.1	Introduction	67
3.2	Discussion and Results	68
3.3	Conclusion	84
3.4	Calculations Methods	85
4	Conductance of Antiaromatic Graphene-like Structures with Different Connectivities	91
4.1	Introduction	91
4.2	Magic numbers for C ₆₀	92
4.3	Conclusion	109
4.4	Calculations Methods	110
5	Theoretical Study of Conductance Ratios for Different Connectivities in C₆₀ Molecule.....	117
5.1	Introduction	117
5.2	Discussion and Results	119
5.3	Conclusion	125
5.4	Calculations Methods	126
6	Conclusions	131

Chapter 1

Molecular electronics

1.1 Introduction

Molecular electronics has attracted great attention from a wide variety of researchers, due to promising applications in nanoscale electronic devices such as transistors [1, 2], switches [3], rectifiers, interconnects [4], organic photovoltaic [5] and chemical sensors [5, 6]. Using molecules as electronic elements has many advantages due to their small sizes, their ability to be self-assemble onto surfaces and the low cost of producing large numbers of identical molecules [7]. However, realizing and controlling the connection between the molecule and electrodes has remained challenging due to small molecular size.

The use of individual molecule as functional electronic devices was first proposed in the 1970s [8]. In order to design and realize molecular devices it is essential to have a good understanding of the properties of an individual molecule. Within the framework of molecular electronics, the most important

property of a molecule is its conductance and the major question in this field is how electrons move through molecules. To address this question, extensive experimental and theoretical studies have been carried out. Various measurement techniques have been developed.

The field is currently attracting attention from a broad cross-section of the scientific community in response to both fascinations with the fundamental scientific challenges associated with the measurement of the electrical properties of molecules, and manipulation of electronic phenomena via molecular processes, and growing concerns over the technological challenges and ultimate limits facing solid state semiconductor technology. The use of organic materials for electronic applications in which the bulk electronic or optoelectronic response arises from ensembles of several millions of molecules, and for which properties are measured or observed on the macroscopic level, is at a mature stage of development and application. The most obvious examples of molecular materials readily available in the electronics mass market are the use of liquid crystals and organic light emitting diodes (OLEDs) in flat video displays. This sector of the electronics industry continues its steady development driven by the promises of transparent, flexible, non-toxic, printable electronics, with improved consumer.

In molecular electronic junctions the electrical signal comes in and out of the molecules via contact-coupled electrodes. The electrodes can be classified as metal or nonmetal electrodes. The development of molecular electronics initially started from the use of metal electrodes. Hence, the development of molecular devices based on metal electrodes will be summarized and then move to those based on nonmetal electrodes, particularly carbon-based electrodes.

- Single-Molecule Junctions

The initial idea of using individual molecules as active electronic elements provided the impetus to develop a variety of experimental platforms to probe their electronic transport properties. Among these platforms, single-molecule junctions based on metal–molecule–metal architecture have received considerable attention and contributed significantly to the fundamental understanding of the physical phenomena required to develop molecular-scale electronic devices. The scanning probe microscopy, SPM, technique is regarded as a milestone in the history of molecular electronics because it has made a great contribution to the development of molecular electronics and continues to promote the advancement of molecular electronics in the future. In addition to SPM technique, Scanning Tunnelling Microscopy Break Junctions (STM-BJ) [9-11] and Mechanically Controllable Break Junctions

MCBJ [12, 13] have been used widely.

In addition to the single-molecule junctions, ensemble molecular junctions, which are formed from more than a few or self-assembled monolayers (SAMs) of molecules, are another important branch of molecular-scale electronics. Currently, there are mainly three universal strategies for forming ensemble molecular junctions for large-area electrical measurements: (1) direct formation of metal electrodes using either electron beam/thermal evaporation or electrochemical deposition, (2) incorporation of electrically conducting polymers/nanomaterials as an electrode, and (3) utilization of liquid metals as electrodes. There are many methods that details the fabrication of ensemble molecular junctions using different state-of-art methods, including lift-and-float, liquid metal contact, nanopore and nanowell, on-wire lithography, nanoimprint lithography, crossbar or crosswire, self-aligned lithog raphy, buffer interlayer-based junctions, and on-edge molecular junctions.

While ordinary metal electrode-based molecular junctions remain operational, different experimental platforms based on nonmetal materials have been constructed, thus leading to new possibilities for molecular-scale electronics. Among these new testing systems, carbon electrode–molecule

junctions, where carbon nanomaterials, including single-walled carbon nanotubes (SWNTs) and graphene, are used as point contacts, are particularly promising because of their unique advantages. First, both the SWNTs and the graphene are molecular chemicals made entirely of sp^2 -hybridized carbon atoms arranged in a honeycomb lattice, thus offering a natural compatibility with organic/biological molecules. Second, these crystalline carbon nanomaterials exhibit extraordinary electronic properties with high stability and chemical flexibility due to their π -conjugated skeletons. Unlike metal electrodes, they are atomically stiff and naturally functional at their ends. When lithographically patterned as point contacts, they are endfunctionalized by carboxylic acid groups. These functional groups could be used to form robust covalent bonds at the molecule/electrode interface through amide linkages that can endure chemical treatments and external stimuli, thus significantly improving the device stability. Third, they are easily available in large areas through bottom-up chemical approaches and can be easily micro-/nanofabricated onto a large range of substrates with high accuracy. Finally, another unique feature of these nanocarbons results from the fact that the low-dimensional nature is molecular in size, ensuring the number of bridged molecules down to the single-molecule level. Because of all of these features, carbon nanomaterials, such as SWNTs and graphene, are

most likely better suited. One of the most important methodologies used to develop robust molecular electronics platforms is Carbon Nanotube-Based Electrodes . Since their discovery in the 1990s, carbon nanotubes have led to a significant amount of research due to their tremendous potential applications in the chemical, physical, and electrical fields. Although they have the simplest chemical composition and atomic bonding configuration, their electronic properties are highly dependent on chirality and diameter. This structural dependence leads to infinite electrical diversity and richness, thus offering unlimited opportunities to tune the energy alignments between the tubes and the molecules of interest. Another efficient strategy to build high-throughput molecular junctions is Graphene-Based Electrodes [14-17]. Graphene, another typical allotropy of carbon, is a two-dimensional zero-band gap semimetal carbon material with extraordinary electronic properties that has received worldwide attention since its discovery by Geim and Novoselov et al. in 2004. Its high mobility and the ease with which it can be doped with either holes or electrons make it suitable as a platform for sensors, electrodes in field-effect transistors, and as transparent contacts for photovoltaic devices.

Generally, materials used as electrodes in molecular junctions should have superior properties in four aspects. (1) The first premise is good electrical

conductivity, which can maintain its high value with dimension scale-down. (2) The second is the stability of the material composition and configuration, which is of great importance for resisting external perturbation/ oxidation and ensuring the success of forming molecular junctions. (3) The third is the abundant availability using either bottom-up or top-down approaches. (4) Last, the fourth is the ease of material processing, which should be compatible with industrial micro/nanofabrication techniques. On the basis of these considerations, the past two decades have witnessed a large variety of materials being used in molecular electronics, ranging from conventional noble metals to novel carbon allotropies, which continuously and creatively update the paradigms for device architecture and operation. In addition to the materials mentioned above, there were also other attempts to expand the research regimes of molecular electronics, including silicon and polymer-based nanoelectrode systems as Silicon-Based Electrodes [18], and CMOS-compatible electrodes, such as Pt and Pd [19].

-Integrating molecular functionalities into electrical circuits.

Undoubtedly, the substantial experimental and theoretical progress detailed above lays the foundation for both the measurement capabilities and a fundamental understanding of the various physical phenomena of molecular

junctions. Despite these considerable achievements, there are still no commercially available molecular electronic devices. To satisfy the requirements for actual applications, the development of practical molecular devices with specific functions is a prerequisite. In fact, recent experimental developments have demonstrated conductance switching/modulation and rectification as well as how quantum interference effects play a critical role in the electronic properties of molecular junctions. The focus of these experiments illustrates the engineering of functionalities that are beyond conventional electronic transport properties using a rational chemical design in single-molecule junctions. In this section, I focus on reviewing the ever-developing trends of integrating molecular functionalities into electrical circuits based on single molecules, which were neglected in most previous reviews, including (1) wiring toward nanocircuits; (2) rectification toward diodes; (3) modulation toward transistors; (4) switching toward memory devices; and (5) transduction toward sensors. For different functions resulted from individual molecules, both molecular “cores” and molecular “tails” are equally important due to the fact that the proposed functions could be affected not only by molecular electrical characteristics but also by the electrode–molecule bonding. Therefore, in each part of this section, we will

pay specific attention to the design of the molecular structures and their influence on the device functions.

In summary, with the rapid development of molecular-scale electronics, using molecular devices as the future of next-generation electrical circuit units with lower power consumption, higher speed, and higher level of integration has received significant attention. To conveniently and efficiently fabricate molecule-based devices, electrode fabrication is a key step. In this report, we presented the developments of different techniques for molecular junction fabrications using both metal and nonmetal materials as contacts. We summarized the characterization methods as well as the theoretical approaches for molecular electronics. Moreover, we highlighted the significant advancements in molecule-based functional devices toward practical applications. The history, challenges, and future of molecular electronics were also discussed. Each type of material and technique has advantages as well as disadvantages. For example, metallic materials are the most widely used materials for the molecular junction fabrication due to their several advantages, such as few defects, low cost, and high conductance. However, from a device's standpoint, several serious concerns for metal nanoelectrodes exist. (1) Incompatibility: Several types of metals (e.g., commonly used gold) may form deep level traps in silicon, making it difficult

to integrate gold tunnel junctions with complementary metal–oxide–semiconductor (CMOS) electronics. (2) Unexpected mobility: The atom at the metal electrode surface may rearrange or move due to the electric field and local heating, especially under ambient conditions, which strongly influence the stability of single-molecule devices. (3) Contact nature: Molecular electronics is often limited by the poorly defined nature of the contact between the molecules and the metal surface. Even for the most well-studied system, such as thiolated molecules on Au contacts, there are no methods to control the types of metal–molecule bonds. Carbon-based electrodes can overcome these problems, for example, incompatibility and unexpected mobility. Using SWNTs as point contacts, well-defined covalent bonds between the electrode and the molecule with a limited number of molecular bonding sites can be created. However, single-molecule studies based on SWNTs also face considerable challenges before they can realize their full commercial application. Because of a lack of precise diameter and chirality control for the SWNTs, the device-to-device properties varied. Developing a reliable fabrication technique for mass-producing identical SWNT arrays and integrating individual SWNTs into functional single-molecule devices with high yields are one of the future challenges. Graphene does not have the inherent variability of the SWNTs and may therefore

circumvent these problems. Graphene is currently considered a potential candidate for the post-CMOS era because its defect-free monolayer can be grown at the wafer scale, and the significant gate screening issues can be reduced as compared to that of metal electrodes, thus putting molecular electronics into a more favorable position due to the junction's dimensions being reduced to two dimensions. Nanometer-scale gaps in graphene have been obtained using different strategies, such as atomic force microscopy nanolithography, anisotropic etching via thermally activated nanoparticles, electron-beam sculpting, lithography, mechanical stress, or electroburning. Functional single-molecule devices based on graphene, such as optical switches with low-ohmic contacts, transistors with low field screening, and ultrasensitive biosensors, have been reported. Carbonbased materials, such as SWNTs and graphene, may be better suited as electrode materials for molecular electronics. The realization of atomic-level precision in the cutting procedure, precise control of the molecular conformation on the substrate within the graphene gaps, and contact configuration are challenges for future studies to overcome. Each electrode fabrication technique has its own unique advantages but is far from perfect. For example, there are main three general techniques for forming top contacts for large-area electrical measurements on the SAMs. (1) Direct deposition of metals using an electron-beam or thermal

evaporation ensures atomic-level contact; however, the device yield is low due to the damage of the evaporated hot metals and the formation of metal filaments that short the junctions. (2) The installation of a buffer-conducting polymer between the SAM and a metallic top contact exhibits a high device yield and efficiently avoids electrical shorts. However, the electrical properties of these molecular junctions may be influenced by the thermal treatment and the morphology of the interlayer conducting films. Also, the interface between the conducting polymer and molecular layer is not well understood. (3) The use of liquid metals allows the formation of the conformal contacts at low cost under room temperature conditions. However, liquid metal has difficulty forming small contacts at the individual molecular level. For single-molecule junctions, single molecules can be addressed using the electromigration method on the nanoconstrictions. However, the electrode separation is fixed, which indicates that the gap size cannot be further changed after electromigration, thus leading to a low yield of molecular junctions. The mechanically controllable junction technique with a precise adjustable gap size indicated a high yield of the junction. However, it is not facile to fabricate highly integrated molecular commercial devices because of the constraint of the out-of-plane push rod components and the difficulty of introducing a third electrode for gating. Each characterization technique has

drawbacks. For example, STM continues to play an important role in understanding the electron transport in single molecules due to its capability for both microscopy and tunneling spectroscopy. However, STM requires well-defined surfaces, such as single crystals, and it is not available for several devices or samples. The surface spectroscopy techniques (e.g., photoemission spectroscopy) are powerful in determining the electronic properties of the molecule–electrode interfaces and the relative energy alignments. X-ray spectroscopy has been demonstrated to provide angstrom-resolution structural information in silicon–molecule–mercury junctions. However, most of the spectroscopic techniques are difficult to apply to molecules sandwiched between two electrodes due to the screen of electrodes. Inelastic electron tunneling spectroscopy can be easily used in sandwiched molecular junctions at the single-molecule level to provide information on molecular identity and conformation. However, it requires cryogenic temperatures to distinguish the vibration modes. Optical techniques, such as infrared and Raman spectroscopies, can be used to probe the chemical properties of molecules at room temperature, but it is still a considerable challenge at the single molecule level. Additionally, although several useful analytical techniques (e.g., transition voltage spectroscopy and thermoelectricity) have been developed for characterizing molecular

junctions, those methods are indirect techniques to reveal the characterization of molecules. Developing new efficient techniques for directly extracting additional details from the molecular junctions is highly expected.

Generally speaking, even after four decades of intensive progress, the molecular electronics field is still very active and thriving. The unique and complicated nature of the transport problem in the open quantum system opens the door for a beautiful future, for fundamental research, and possible device application development.

1.2 Thesis Outline

In this thesis, I mainly focus on single molecule transport properties of molecules including moieties such as furan, pyrrole, thiophene, cyclopentadiene, tris(benzocyclobutadieno)triphenylene, biphenylene and C₆₀ molecule. Chapter 2 includes a general description of some basic subjects related to single molecule transport theory involving the Schrodinger equation, the Landauer formula, Green's functions for different transport regimes, resonant transport, the magic ratio rule and the counterpoise method to calculate binding energy. Chapter 3 presents a theoretical and experimental study of the synergistic effects of molecular symmetry and quantum interference on the charge transport through single-molecule junctions with

five-membered core rings using pyridyl anchoring groups. Further theoretical calculations using thiol anchoring groups are presented. At the end of this chapter, the binding energies of the five membered compounds (symmetric and asymmetric compounds) are computed to explore how they are affected by molecular symmetry. In chapter 4, the main goal is to examine the validity of the magic ratio rule (introduced in chapter 2) when applied to antiaromatic graphene-like molecules using two molecules tris(benzocyclobutadieno)triphenylene and biphenylene with a comparison between the transmission coefficients of different components is presented. Chapter 5 gives a theoretical study of the transport properties of C_{60} involving an examination of the validity of the magic ratio rule for such a non-aromatic molecule. Finally, conclusions will be presented in chapter 6.

References

1. Martel, R., et al., *Single- and multi-wall carbon nanotube field-effect transistors*. Applied Physics Letters, 1998. **73**(17): p. 2447-2449.
2. DeHon, A., *Array-based architecture for FET-based, nanoscale electronics*. IEEE Transactions on Nanotechnology, 2003. **2**(1): p. 23-32.
3. Donhauser, Z.J., et al., *Conductance Switching in Single Molecules Through Conformational Changes*. Science, 2001. **292**(5525): p. 2303.
4. Wang, C., et al., *Ultrathin Au nanowires and their transport properties*. J Am Chem Soc, 2008. **130**(28): p. 8902-3.
5. Tsutsui, M. and M. Taniguchi, *Single Molecule Electronics and Devices*. Sensors (Basel, Switzerland), 2012. **12**(6): p. 7259-7298.
6. Waser, R. and M. Aono, *Nanoionics-based resistive switching memories*. Nature Materials, 2007. **6**: p. 833.
7. Franzon, P., et al., *Molecular Electronics – Devices and Circuits Technology*, in *Vlsi-Soc: From Systems To Silicon: Proceedings of IFIP TC 10, WG 10.5, Thirteenth International Conference on Very Large Scale Integration of System on Chip (VLSI-SoC 2005), October 17-19, 2005, Perth, Australia*, R. Reis, A. Osseiran, and H.-J. Pfleiderer, Editors. 2007, Springer US: Boston, MA. p. 1-10.

8. Petty, M.C., et al., *Molecular Electronics*, in *Springer Handbook of Electronic and Photonic Materials*, S. Kasap and P. Capper, Editors. 2017, Springer International Publishing: Cham. p. 1-1.
9. C-S. Wang, A S. Batsanov, M. R. Bryce, S. Martin, R. J. Nichols, S. J. Higgins, V. M. García-Suárez and C. J. Lambert, Oligoynes Single Molecule Wires, *Journal of the American Chemical Society* 131, 15647 (2009)
10. E. Leary, H. Höbenreich, S. J. Higgins, H. van Zalinge, W. Haiss, R.J. Nichols, C. Finch, I. Grace and C.J. Lambert, Single-molecule, solvation-shell sensing, *Phys Rev. Lett.* 102, 086801 (2009)
11. GJ Ashwell, B Urasinska, C Wang, MR Bryce, I Grace, CJ Lambert, “Single-molecule electrical studies on a 7 nm long molecular wire” *Chemical Communications*, 4706-4708 2006
12. Huber, R.; Gonzalez, M. T.; Wu, S.; Langer, M.; Grunder, S.; Horhoiu, V.; Mayor, M.; Bryce, M. R.; Wang, C. S.; Jitchati, R.; Schonenberger, C.; Calame, M. J. *Am. Chem. Soc.* 2008, 130, 1080-1084.
13. Hong, W.; Manrique, D. Z.; Moreno-García, P.; Gulcur, M.; Mishchenko, A.; Lambert, C. J.; Bryce, M. R.; Wandlowski, T. J. *Am. Chem. Soc.* 2011, 134, 2292-2304.

14. H Sadeghi, JA Mol, CS Lau, GAD Briggs, J Warner, CJ Lambert, “Conductance enlargement in picoscale electroburnt graphene nanojunctions,” *Proceedings of the National Academy of Sciences* 112 (9), 2658-2663, 2015
15. JA Mol, CS Lau, WJM Lewis, H Sadeghi, C Roche, A Cnossen, JH Warner, C.J. Lambert, H.L. Anderson and G.A.D. Briggs, “Graphene-porphyrin single-molecule transistors,” *Nanoscale* 7 (31), 13181-13185, 2015
16. XH Zheng, GR Zhang, Z Zeng, VM García-Suárez, CJ Lambert, “Effects of antidots on the transport properties of graphene nanoribbons,” *Physical Review B* 80 (7), 075413, 2009
17. H Sadeghi, S Sangtarash, CJ Lambert, “Enhancing the thermoelectric figure of merit in engineered graphene nanoribbons” *Beilstein journal of nanotechnology* 6, 1176 2015
18. H Sadeghi, S Bailey, CJ Lambert, “Silicene-based DNA nucleobase sensing,” *Applied Physics Letters* 104 (10), 103104 2014
19. VM García-Suárez, AR Rocha, SW Bailey, CJ Lambert, S Sanvito, J Ferrer, “Single-channel conductance of H₂ molecules attached to platinum or palladium electrodes,” *Physical Review B* 72 (4), 045437, 2005

20. CM Finch, S Sirichantaropass, SW Bailey, IM Grace, VM Garcia-Suarez, C J Lambert, “Conformation dependence of molecular conductance: chemistry versus geometry,” *Journal of Physics: Condensed Matter* 20 (2), 022203 2007
21. Laura Rincón-García, Ali K Ismael, Charalambos Evangelis, Iain Grace, Gabino Rubio-Bollinger, Kyriakos Porfyrakis, Nicolás Agrait, Colin J Lambert “Molecular design and control of fullerene-based bi-thermoelectric materials” *Nature materials* 15 (3), 289-293 (2016)
22. Yonghai Li, Masoud Baghernejad, Al-Galiby Qusiy, David Zsolt Manrique, Guanxin Zhang, Joseph Hamill, Yongchun Fu, Peter Broekmann, Wenjing Hong, Thomas Wandlowski, Deqing Zhang, CJ Lambert, “Three-State Single-Molecule Naphthalenediimide Switch: Integration of a Pendant Redox Unit for Conductance Tuning” *Angewandte Chemie International Edition* 54 (46), 13586-13589 2015
23. VM García-Suárez, CJ Lambert, DZ Manrique, T Wandlowski, “Redox control of thermopower and figure of merit in phase-coherent molecular wires,” *Nanotechnology* 25 (20), 205402 2014

Chapter 2

Single Molecule Transport Theory

2.1 Introduction

Electrical conductance is one of the most important properties of single molecules in the field of molecular electronics. Many theoretical descriptions of electron transport properties (including conductance) through single molecule systems are based on the Landauer formula, which is a simple expression for the relation between the transmission probability of the electron and the electronic conductance in one-dimensional structures with two terminals. The Landauer formula was later generalized by Buttiker to the case of multi-terminal devices. According to the Landauer formalism, the conductance can be calculated from a transmission probability, which in turn can be evaluated using Green's functions.

In this chapter, I will start with a brief overview of Schrodinger equation and then Landauer and Buttiker formulas. Then I will discuss scattering theory and Green's functions for different transport regimes. As an example, a one dimensional structure with an arbitrarily scattering region will be used to

present the general methodology used to describe the transmission coefficient $T(E)$ in a molecular junction for electrons with energy E traversing from one electrode to another. Thereafter different types of resonances will be discussed that characterize the conductance within a general theory of electronic transport. Then, I will introduce the magic ratio rule (MRR) method that I use to predict the conductance ratios [1]. Finally, counterpoise method to calculate binding energy will be represented.

2.2 Schrodinger equation

The Schrodinger equation is one of the fundamental equations in non-relativistic quantum mechanics. It describes the time evolution of a quantum state in atomistic or molecular configurations and was proposed in 1926 by the Austrian physicist Erwin Schrodinger. The Schrodinger equation can be written in two different forms, the time dependent Schrodinger equation and the time independent Schrodinger equation. The time dependent Schrodinger equation is the most general form which gives a description of a system evolving with time where the time independent Schrodinger equation is sufficient when the systems in a stationary state. The most general

Schrodinger equation describes the evolution of the physical properties of a system in time is:

$$i\hbar \frac{\partial}{\partial t} \psi(r, t) = \hat{H}\psi(r, t) \quad (2.1)$$

Where, ψ is the wave function, of the quantum system, and \hat{H} is the Hamiltonian operator which characterizes the total energy of any given wave function and \hbar is the reduced Planck constant ($h/2\pi$).

For a single particle in a potential,

$$i\hbar \frac{\partial}{\partial t} \psi(r, t) = \left(-\frac{\hbar^2}{2m} \nabla^2 + U(r, t) \right) \psi(r, t) \quad (2.2)$$

Separating the variables, where $\psi(r, t) = \psi(r)f(t)$, the Schrodinger equation then turns to two ordinary differential equations:

$$\frac{1}{f(t)} \frac{d}{dt} f(t) = -\frac{iE}{\hbar} \quad (2.3)$$

and

$$\hat{H}\psi(r) = E\psi(r) \quad (2.4)$$

Thus,

$$f(t) = e^{-iEt/\hbar} \quad (2.5)$$

Then, the time dependent Schrodinger equation solution is obtained:

$$\psi(r, t) = \psi(r)e^{-iEt/\hbar} \quad (2.6)$$

Where, the most general solution is:

$$\psi(r, t) = \sum_i c_i \psi_i(r) e^{-iEt/\hbar} \quad (2.7)$$

Equation 2.4 represents the time-independent Schrodinger equation which has the form of an eigenvalue equation.

2.3 The Landauer formula

The Landauer formula [2, 3] was first suggested by Rolf Landauer in 1957 [4] for two terminals. To illustrate the formula, consider a scattering region connected to two electrodes (leads) as sketched in Figure 2.1. The leads are assumed to be ballistic conductors, i.e. conductors with no scattering and thus the transmission probability equals one [5]. Each lead, in turn, is coupled to a reservoir where all inelastic processes take place. Suppose that the chemical

potentials of the reservoirs on the left and right hand sides are μ_l, μ_r respectively, and let the temperature be equal to zero ($T = 0 K$).

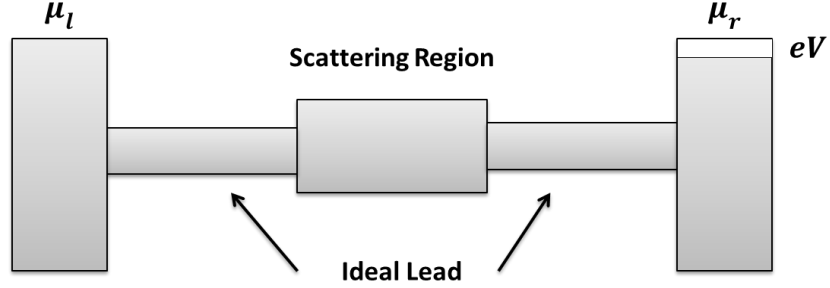


Figure 2.1: Schematic view of a 1D scattering region connected to two reservoirs with different chemical potentials μ_l and μ_r via ideal leads.

Consider the case of a 1-dimensional system. When the scattering region is an ideal 1-dimensional lead, so that the two reservoirs are connected by a perfect 1-d lead with no scattering, the current through this system, which flows due to the chemical potential difference between the reservoirs is ,

$$I = (-e)v \frac{\partial n}{\partial E} (\mu_l - \mu_r) \quad (2.8)$$

Here v is the group velocity, e is the electronic charge and $\partial n / \partial E$ is the density of states per unit length of the electrons which is given by $\partial n / \partial E = 1 / \pi \hbar v$. It is worth mentioning that the Landauer formula describes the linear response conductance, hence it only holds for small bias voltages, $\delta V \rightarrow 0$. Thus,

$$I = \frac{-e}{\pi\hbar}(\mu_l - \mu_r) \quad (2.9)$$

In the presence of the scatter, these electrons have a transmission probability T to traverse the scattering region, therefore, the current flow is:

$$I = \frac{-2e}{h}T(\mu_l - \mu_r) \quad (2.10)$$

Since the chemical potentials difference between the reservoirs is given by $-eV = \mu_l - \mu_r$, the conductance between the two terminals is obtained as:

$$G = \frac{I}{V} = \frac{2e^2}{h}T = G_0T \quad (2.11)$$

Where $G_0 = \frac{2e^2}{h}$. This relation is called Landauer formula for a one-dimensional system [2, 3]. For a perfect conductor where $T = 1$, the Landauer formula becomes:

$$G = G_0 \approx 12.9 (k\Omega)^{-1} \quad (2.12)$$

Where, G_0 , is the conductance quantum.

At a finite temperature the Landauer formula (2.10) is transformed into the more general formula for the current [4]:

$$I = \frac{2e}{h} \int T(E) [f(E - \mu_l) - f(E - \mu_r)] dE \quad (2.13)$$

Where f is the Fermi-Dirac distribution $f(E - \mu) = 1/(1 + e^{(E-\mu)/k_B T})$ related to the chemical potential μ , T is temperature and k_B is Boltzmann's constant. In the case of the linear response regime (i.e. at low bias eV), the Fermi-Dirac functions in eq. (2.13) can be Taylor expanded around the Fermi energy [5] resulting in:

$$I = \frac{2e^2 V}{h} \int_{-\infty}^{+\infty} dE T(E) \left[-\frac{\partial f(E)}{\partial(E)} \right] \quad (2.14)$$

Last equation shows that when the voltage is small, the current is linearly proportional to the voltage, and then we can write:

$$I = GV \quad (2.15)$$

Where G is the conductance of the two terminals device. Thus:

$$G = G_0 \int_{-\infty}^{+\infty} dE T(E) \left[\frac{-\partial f(E)}{\partial(E)} \right] \quad (2.16)$$

As mentioned above, the current in equation (2.15) is linearly proportional to the voltage and because of this linearity, this system of transport is called linear response regime.

2.4 Landauer-Buttiker formalism

Landauer original result was obtained for two-terminal systems and then its idea was extended by Buttiker to the case of multi-terminal devices where the matrix form of the full formalism including the transmission probability is needed. Buttiker suggested that the Landauer formula, equation (2.10), can be generalized to structure with many terminals by writing the current I_i at the i th terminal as [6]:

$$I_i = \frac{-2e}{h} \sum_j (T_{ji} \mu_i - T_{ij} \mu_j) \quad (2.17)$$

Where $T_{ji}(T_{ij})$ is the transmission probability from terminal j (i) to terminal i (j). We therefore define:

$$G_{ij} = G_0 T_{ij} \quad (2.18)$$

And rewrite Eq. (2.17) as:

$$I_i = \sum_j (G_{ji} \mu_i - G_{ij} \mu_j) \quad (2.19)$$

Current conservation gives some conditions for currents and conductance, because

$$\sum_i I_i = 0 \quad (2.20)$$

Furthermore all currents should be zero, when the potential μ_i of all the terminals are equal:

$$\sum_j (G_{ji} - G_{ij}) = 0 \quad (2.21)$$

This allows us to rewrite equation (2.19) as:

$$I_i = \sum_j G_{ij} (\mu_i - \mu_j) \quad (2.22)$$

This is the so-called Landauer-Buttiker formula for the multi-terminal structures.

2.5 Green's Functions

Green's function (GF) is a useful tool for studying the properties of nano-scale structures because it can be used to express all of the observable properties of the system of interest [7]. In this section I will first discuss how to construct the Green's function for some separate lattices. Then I will briefly discuss how to connect the Green's functions of these separable

lattices together to construct the Green's function of the whole system using Dyson equation.

2.5.1 Green's function of doubly infinite chain

In this section I will derive the one dimensional doubly infinite Green's function of the electrodes, where these electrodes are described as a perfect one dimensional chain as shown in Figure 2.2 In order to obtain the scattering amplitudes we need to calculate the Green's function of the system.

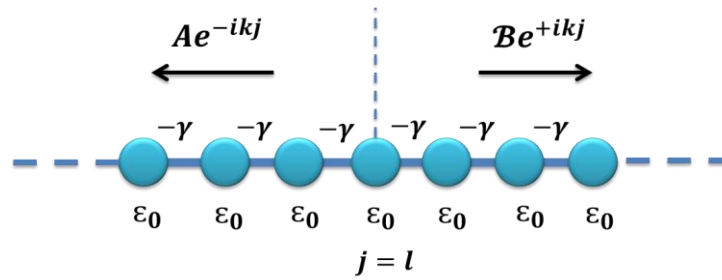


Figure 2.2: Tight-binding representation of a one-dimensional infinite lattice with on-site energies ϵ_0 and couplings $-\gamma$.

The Green's function for a system obeying the Schrodinger's equation

$$(E - H)\psi = 0 \quad (2.23)$$

is defined as:

$$(E - H)G = I \quad (2.24)$$

The solution for this equation can be written as:

$$G = (E - H)^{-1} \quad (2.25)$$

Where, G , is the retarded Greens function g_{jl} , describes the response of a system at a point j due to a source at l . This source causes excitation which raises two waves, travelling to the left and right as shown in Figure 2.2.

Where,

$$g_{jl} = \begin{cases} Ae^{-ikj} & , \quad j < l \\ Be^{+ikj} & , \quad j > l \end{cases} \quad (2.26)$$

Here, A and B are the amplitudes of the two outgoing waves travelling to the left and right, respectively. Green's function must be continuous at $j = l$. As a result we can write:

$$g_{jl}|_{j=l} = \begin{cases} Ae^{-ikl} & , \text{let } \dots A = Ce^{+ikl} \\ Be^{+ikl} & , \text{let } \dots B = Ce^{-ikl} \end{cases} \quad (2.27)$$

Therefore:

$$Ae^{-ikl} = Be^{+ikl} = C \quad (2.28)$$

Substituting from equation (2.28) into equation (2.26) results in:

$$g_{jl} = Ce^{ik|j-l|} \quad (2.29)$$

In order to obtain the constant C , equation (2.24) has to be satisfied using equation (2.29), thus:

$$C = \frac{1}{2i\gamma \sin k} = \frac{1}{i\hbar v} \quad (2.30)$$

Combining the last two equations yields:

$$g_{jl} = \frac{e^{ik|j-l|}}{i\hbar v} \quad (2.31)$$

This equation represents Green's function of a doubly infinite one-dimensional chain [5, 8, 9].

2.5.2 Green's function of semi-infinite one-dimensional chain

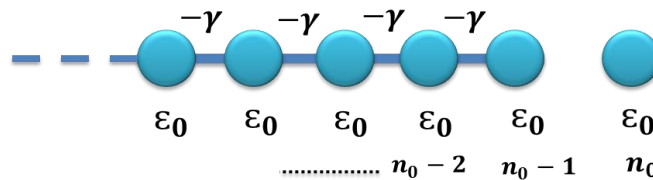


Figure 2.3: Tight-binding representation of a one-dimensional semi-infinite lattice with on-site energies ϵ_0 and couplings $-\gamma$.

In order to obtain Green's function of a semi-infinite chain from Green's function of a doubly infinite chain, an appropriate boundary condition should

be introduced. Let consider one dimensional lattice with site energies ε_0 and hopping elements $-\gamma$ as shown in Figure 2.3. The chain must be terminated at a given point, n_0 so all points for which $n \geq n_0$ are missing, that means that the Green's function should vanish at site n_0 . This can be achieved by adding a wave function to the Green's function of the doubly infinite chain. The proper wave function in this case is:

$$\psi_{jl} = -\frac{e^{-ik(j+l-2n_0)}}{i\hbar v} \quad (2.32)$$

Therefore:

$$g_{jl} = \frac{e^{ik|j-l|}}{i\hbar v} - \frac{e^{-ik(j+l-2n_0)}}{i\hbar v} \quad (2.33)$$

Satisfying the boundary condition ($j = l = n_0 - 1$) yields:

$$g_{n_0-1, n_0-1} = \frac{1}{i\hbar v} - \frac{e^{2ik}}{i\hbar v} \quad (2.34)$$

Hence, the Green's function at site $j=n_0-1$ due to a source at site $l=n_0-1$ is:

$$g_{n_0-1, n_0-1} = -\frac{e^{ik}}{\gamma} \quad (2.35)$$

2.5.3 Green's function of a finite one-dimensional chain

To derive the Green's function of a finite one-dimensional lattice, consider a linear chain of N atoms as expressed in Figure 2.4. Green's function should vanish at site $n=0$ and site $n=N+1$.

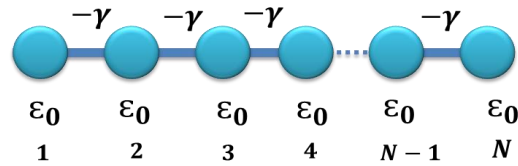


Figure 2.4: Tight-binding representation of a one-dimensional semi-infinite lattice with on-site energies ϵ_0 and couplings $-\gamma$.

To achieve that, Green's function should take the following expressions:

$$g_{jl} = \begin{cases} A \sin kj & , \quad j < l \\ B \sin k(j - (N + 1)) & , \quad j > l \end{cases} \quad (2.36)$$

So the boundary conditions will be satisfied. The Green's function must be continuous at $j = l$, so

$$g_u = \begin{cases} A \sin kl & , A = C \sin k(l - (N + 1)) \\ B \sin k(l - (N + 1)) & , B = C \sin kl \end{cases} \quad (2.37)$$

Therefore:

$$g_{jl} = \begin{cases} C \text{sinc}(l - (N + 1)) \text{sinc} j & , \quad j \leq l \\ C \text{sinc} l \text{sinc}(j - (N + 1)) & , \quad j \geq l \end{cases} \quad (2.38)$$

Then C can be obtained as:

$$C = \frac{1}{\gamma \text{sinc} \text{sinc}(N + 1)} \quad (2.39)$$

This gives the Green's function of a finite one-dimensional chain containing atom 1 and N at the opposite ends:

$$g_{N1} = \frac{-\text{sinc}}{\gamma \text{sinc}(N + 1)} \quad (2.40)$$

2.5.4 One dimensional scattering

To construct the Green's function of the whole system we have to connect the Green's functions of the separable lattices together. Let us first consider the case of decoupled leads ($\alpha = 0$) shown in Figure 2.5. The total Green's function of the system can be given by the decoupled Green's function:

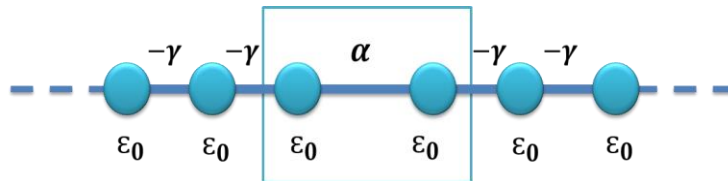


Figure 2.5: Tight-binding representation of a one dimensional scattering region attached to one dimensional leads.

$$g = \begin{pmatrix} e^{ik} & 0 \\ -\frac{e^{ik}}{\gamma} & 0 \\ 0 & -\frac{e^{ik}}{\gamma} \end{pmatrix} = \begin{pmatrix} g_L & 0 \\ 0 & g_R \end{pmatrix} \quad (2.41)$$

For the case of coupled system, Green's function of the whole system can be obtained using Dyson's equation:

$$G = (g^{-1} - V)^{-1} \quad (2.42)$$

Here the operator V describes the interaction connecting the two leads and has the form:

$$V = \begin{pmatrix} 0 & V_c \\ V_c^\dagger & 0 \end{pmatrix} = \begin{pmatrix} 0 & \alpha \\ \alpha^* & 0 \end{pmatrix} \quad (2.43)$$

The solution to Dyson's equation is:

$$G = \frac{1}{\gamma^2 e^{-2ik} - \alpha^2} \begin{pmatrix} -\gamma e^{-ik} & \alpha \\ \alpha^* & -\gamma e^{-ik} \end{pmatrix} \quad (2.44)$$

This expression is Green's function for the whole system under consideration.

2.6 Transport through an arbitrary scattering region

As mentioned previously, once the Green's function is calculated the transmission probability is easy to obtain. In this section I will derive the most general formula for the transmission probability for an arbitrarily shaped scattering structure. Here I will use a different approach starting with the wave functions leading to the surface Green's function and ending up with a general formula for the transmission probability.

Considering the system in Figure 2.6, where an arbitrary scattering region with Hamiltonian H is connected to two one dimensional leads. On-site energies of the left and right leads are ϵ_0 and the coupling in the two leads is $-\gamma$.

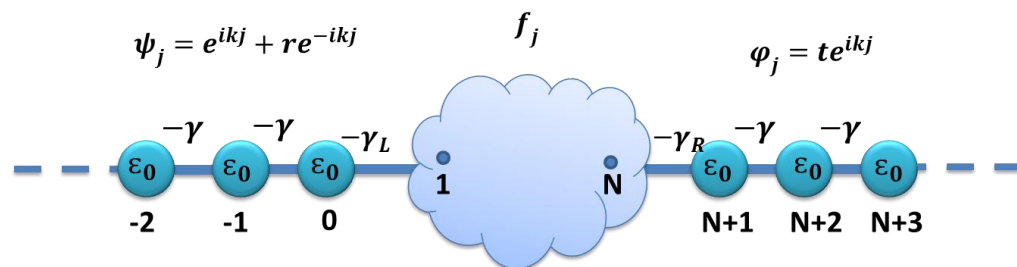


Figure 2.6: Tight-binding representation of a one dimensional arbitrarily scattering region attached to one dimensional leads.

The leads are connected to the site (1) and (2) of the scattering region with the couplings $-\gamma_L$ and $-\gamma_R$. The Hamiltonian for this system is:

$$\begin{bmatrix} \varepsilon_0 & -\gamma & 0 & 0 & 0 & 0 & 0 \\ -\gamma & \ddots & \ddots & 0 & 0 & 0 & 0 \\ 0 & \ddots & \varepsilon_0 & -\gamma_L & 0 & 0 & 0 \\ 0 & 0 & -\gamma_L & \mathbf{h} & -\gamma_R & 0 & 0 \\ 0 & 0 & 0 & -\gamma_R & \varepsilon_0 & \ddots & 0 \\ 0 & 0 & 0 & 0 & \ddots & \ddots & -\gamma \\ 0 & 0 & 0 & 0 & 0 & -\gamma & \varepsilon_0 \end{bmatrix}$$

If the wave function in the left, the right and the scattering region are $\psi_j = e^{ikj} + re^{-ikj}$, $\varphi_j = te^{ikj}$ and f_j , respectively, the Schrodinger equations in left, right, scattering region and connection points could be written as:

$$\varepsilon_0\psi_j - \gamma\psi_{j-1} - \gamma\psi_{j+1} = E\psi_j \quad \text{for } j \leq -1 \quad (2.45)$$

$$\varepsilon_0\psi_0 - \gamma\psi_{-1} - \gamma_L f_1 = E\psi_0 \quad \text{for } j = 0 \quad (2.46)$$

$$\sum_{j=1}^N h_{ij} f_j - \gamma_L \psi_0 \delta_{i1} - \gamma_R \varphi_{N+1} \delta_{iN} = E f_i \quad \text{for } 0 \leq j \leq N + 1 \quad (2.47)$$

$$\varepsilon_0\varphi_{N+1} - \gamma_R f_N - \gamma\varphi_{N+2} = E\varphi_{N+1} \quad \text{for } j = N + 1 \quad (2.48)$$

$$\varepsilon_0 \varphi_j - \gamma \varphi_{j-1} - \gamma \varphi_{j+1} = E \varphi_j \quad \text{for } j > N + 1 \quad (2.49)$$

Equation 2.47 could be re-written as $|f\rangle = g|x\rangle$ where $g = (E - H)^{-1}$ is the Green's function and $|x\rangle$ called source which is a zero vector with non-zero elements only in the connection points at site $j = 0$ and $j = N + 1$, $|f\rangle$, has only two non-zero elements due to the source,

$$\begin{pmatrix} f_1 \\ f_N \end{pmatrix} = \begin{pmatrix} g_{11} & g_{1,N} \\ g_{N,1} & g_{N,N} \end{pmatrix} \begin{pmatrix} x_0 \\ x_{N+1} \end{pmatrix} \quad (2.50)$$

Where $x_0 = \gamma_L \psi_0$ and $x_{N+1} = \gamma_R \varphi_{N+1}$.

Using recurrence relation gives:

$$\gamma \varphi_N = \gamma_R f_N \quad (2.51)$$

$$\gamma \psi_1 = \gamma_L f_1 \quad (2.52)$$

$$\varphi_N = \varphi_{N+1} e^{-ik} \quad (2.53)$$

$$\psi_1 = 2i \sin k + e^{-ik} \psi_0 \quad (2.54)$$

Combining last four equations with equation (2.50) gives:

$$\begin{pmatrix} -g_{11}\gamma_L - \frac{\gamma}{\gamma_L} e^{-ik} & -g_{1N}\gamma_R \\ -g_{N1}\gamma_L & -g_{NN}\gamma_R - \frac{\gamma}{\gamma_R} e^{-ik} \end{pmatrix} \begin{pmatrix} \psi_0 \\ \varphi_{N+1} \end{pmatrix} = \frac{\gamma}{\gamma_L} 2i \operatorname{sinc} \begin{pmatrix} 1 \\ 0 \end{pmatrix} \quad (2.55)$$

Thus:

$$\begin{pmatrix} \psi_0 \\ \varphi_{N+1} \end{pmatrix} = 2i \operatorname{sinc} \frac{\gamma}{\gamma_L} \frac{1}{d} \begin{pmatrix} -g_{NN}\gamma_R - \frac{\gamma}{\gamma_R} e^{-ik} \\ -g_{N1}\gamma_L \end{pmatrix} \quad (2.56)$$

Therefore the transmission t and reflection r amplitudes could be obtained.

$$t = iv \left[\gamma_L g \left(\frac{g_{N1}}{\Delta} \right) \gamma_R g \right] \quad (2.57)$$

Where

$$g = -\frac{e^{ik}}{\gamma} \quad (2.58)$$

is the Green's function of semi-infinite chain and

$$\Delta = 1 - \Sigma_L g_{11} - \Sigma_R g_{NN} + \Sigma_L \Sigma_R (g_{11} g_{NN} - g_{N1} g_{1N})$$

Where, $\Sigma_{L,R} = \gamma_{L,R}^2 g$ are the self energies due to the left and right contact.

The transmission probability is $T(E) = |t|^2$ then:

$$T(E) = v^2 \left[\left(\frac{\gamma_L}{\gamma} \right)^2 \frac{|g_{N1}|^2}{|\Delta|^2} \left(\frac{\gamma_R}{\gamma} \right)^2 \right] \quad (2.59)$$

This is the most general formula to calculate the transmission probability for any scattering region connected to identical leads.

2.7 Features of the Transport Curve

The main feature of electron transport through single molecules and phase-coherent nanostructures is the appearance of transport resonances associated with quantum interference. Deep understanding of the transmission process can be achieved by looking at the properties of these resonances. Here, I will briefly discuss different kinds of resonances, including Breit–Wigner resonances [10], anti-resonances [11, 12], and Fano resonances [13, 14].

2.7.1 Breit-Wigner resonance

For electrons of energy E passing through a single molecular orbital, the transmission probability could be expressed by a Lorentzian function, via the Breit-Wigner formula:

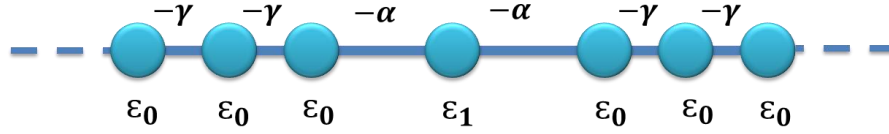


Figure 2.7: Tight binding model to possessing a Breit-Wigner resonance. Two one-dimensional semi-infinite chains coupled to a scattering region of site energy ϵ_0 by hopping elements $-\gamma$

$$T(E) = \frac{4\Gamma_1\Gamma_2}{[(E - \epsilon_n)^2 + (\Gamma_1 + \Gamma_2)^2]} \quad (2.60)$$

Within this formula, the transmission coefficient $T(E)$ of the single molecular junction can be described by two parameters: (Γ) and (ϵ_n) where (Γ) is the strength of the coupling between the molecule and the electrodes (labeled 1 and 2) and $\epsilon_n = E_n - \Sigma$ is the eigen energy E_n of the molecular orbital shifted slightly by an amount Σ due to the coupling of the orbital to the electrodes. Transmission coefficient $T(E)$ has Breit-Wigner-type resonances showing the maximum value when the electron resonates with the molecular orbital (i.e. when $E = \epsilon_n$). Figure 2.7 shows a scattering region with a single impurity placed between two one-dimensional semi-infinite chains. Where, Figure 2.10 shows the tight binding representation of the transmission probability (blue curve) for this system. The formula is valid

when the energy E of the electron is close to an eigen energy E_n of the isolated molecule, and if the level spacing of the isolated molecule is larger than $(\Gamma_1 + \Gamma_2)$. In the case of a symmetric molecule attached symmetrically to identical leads (i.e. $\Gamma_1 = \Gamma_2$ and again when $(E = \varepsilon_n)$, $T(E)$ equals one. The width of the resonance depends on the coupling component α where if the coupling element α is large, the resonances are wider.

2.7.2. Fano resonances

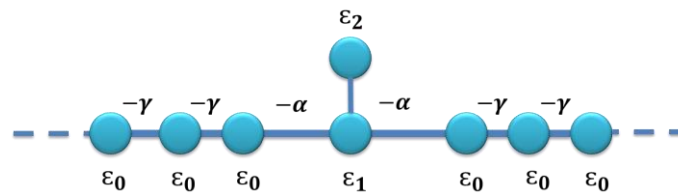


Figure 2.8: Tight binding model to study Fano resonances. Two one-dimensional semi-infinite chains coupled to a scattering region of site energy ε_0 by hopping elements $-\gamma$ where an extra energy level is attached to the scattering region.

In contrast to the Breit-Wigner resonance (a symmetric shape line); Fano resonance was explained as a phenomenon of constructive and destructive interferences between a bound state and the continuum where the corresponding spectral lines are asymmetric. For example, a molecule with a side group produces a Fano resonance when the energy E of the incident electron is close to an energy level in the side group. Fano resonances have

been observed in various systems including quantum dots, nanowires, tunnel junctions and more. Figure 2.8 expresses a simple example of a system contains two one-dimensional semi-infinite chains with site energies ϵ_0 and hopping elements $-\gamma$ coupled to a scattering region with two site energies ϵ_1 and ϵ_2 . The red curve in Figure 2.10 shows the transmission probability for this system using tight binding.

2.7.3. Anti-Resonances

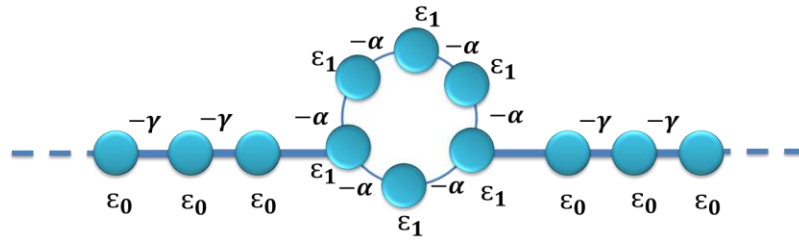


Figure 2.9: Tight binding model to study anti-resonance. Two one-dimensional semi-infinite chains coupled to the scattering region.

This kind of resonance appears in the transmission probability spectrum when the system is multi-branched and destructive interference occurs between propagating waves. A simple example is shown in Figure 2.9, where two one-dimensional semi-infinite chains with site energies ϵ_0 and hopping

elements $-\gamma$ are coupled to a scattering region with six site energies (ϵ_1). The magenta curve in Figure 2.10 shows the general shape of the transmission probability related to this kind of resonance.

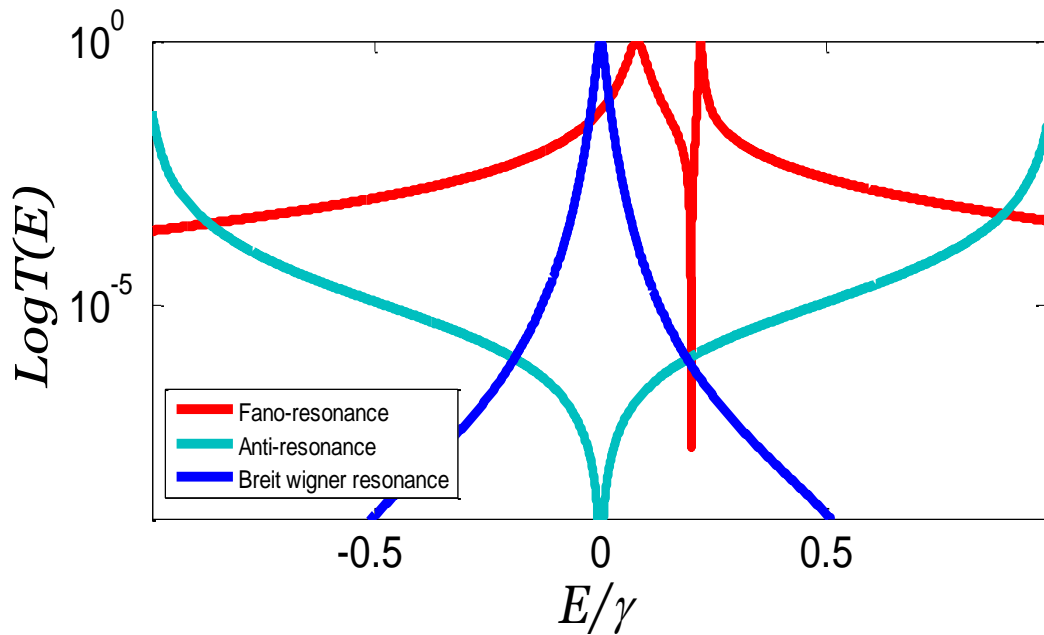


Figure 2.10: Tight binding representation of the transmission coefficients for the above systems showing different kind of resonances.

2.8 The Magic Ratio Rule

For polycyclic aromatic hydrocarbons (PAHs), in the co-tunneling regime, where a single molecule is weakly connected to ‘compound electrodes’ via sites i and j , electrons passing through the molecule from one electrode to the other can

remain phase coherent, even at room temperature [15, 16]. This means that quantum interference QI will determine the electrical conductance of single molecules [17, 18], as was confirmed in a series of recent experiments revealing room-temperature signatures of QI [19, 20]. These signatures are described by counting rules [21, 22] which identify conditions for the occurrence of *destructive* quantum interference, while recently-developed mid-gap theory and magic numbers can be used to account for constructive interference [23 ,1].

The “Magic ratio rule” is based on tables of magic numbers M_{ij} , called M-tables, which capture the contribution of connectivity to the electrical conductance of graphene-like aromatic molecules. They allow the prediction of conductance ratios via this rule, which states that “the ratio of conductances of two molecules is equal to the square of the ratio of their magic integers”.

In references [24 ,1], it is noted that provided electrodes are weakly coupled to the central core, the electrical conductance σ_{ij} of such a junction can be written as a product of the form

$$\sigma_{ij} = V_1 \tau_{ij} V_2, \quad (2.61)$$

where the connectivity-independent terms V_1 and V_2 are random numbers associated with the unknown shapes and binding to the electrodes, while τ_{ij} is a

non-random contribution from the central core, which depends on the connectivity i,j . The validity of equation (2.61) and the theoretical discussion below requires that the Fermi energy of the gold should lie within the HOMO-LUMO gap of the central core, so that transport takes place via phase-coherent co-tunneling and multiple scattering effects between the core and virtual electrodes are suppressed [23]. Equation (2.61) is significant, because it suggests that the ratios of experimentally-reported “statistically-most-probable conductances” corresponding to different connectivities i,j and l,m are properties of the core of the molecule and satisfy

$$\frac{\sigma_{ij}}{\sigma_{lm}} = \frac{\tau_{ij}}{\tau_{lm}} \quad (2.62)$$

which allows one to predict conductance ratios from a knowledge of the core alone[4]. For PAH cores refs [23,1], it was also demonstrated that the effect of connectivity on the core transmissions τ_{ij} can be calculated by introducing tables of ‘magic numbers’ M_{ij} , and the resulting theory was termed ‘analytic M-theory’. From these M-tables one obtains $\tau_{ij} = (M_{ij})^2$. Conceptually, M-theory is a minimal description of connectivity-driven electron transport, whose simplicity arises from the fact that it is restricted to predicting conductance ratios rather than individual conductances.

A crucial quantity in M-theory is the value of the Fermi energy E_F of the electrodes relative to the middle of the HOMO-LUMO gap of the molecule, which henceforth refers to as simply ‘the Fermi energy’. Remarkably for PAHs, it is shown that under the assumption that E_F coincides with the middle of the HOMO-LUMO gap, the predicted conductance ratios are in close agreement with experiment [1, 20, 23].

It should be noted that the MRR predicts ratios of statistically-most-probable conductances. Indeed equation (2.61) allows us isolate the statistical fluctuations due to variability of the molecule-gold contacts from the properties of the core. For example, in experiments using mechanically-controlled break junctions, this variability is overcome by creating histograms of the logarithmic conductance $L_{ij}(V_1, V_2) = \log_{10}\sigma_{ij}$ from thousands of conductance measurements and reporting the statistically-most probable value $\bar{L}_{ij}(V_1, V_2)$, or alternatively the conductance $\bar{\sigma}_{ij} = 10^{\bar{L}_{ij}(V_1, V_2)}$. Since this variability arises from fluctuations in V_1 and V_2 , equation (2.61) yields

$$\bar{L}_{ij}(V_1, V_2) = \log_{10}\bar{\sigma}_{ij} = \log_{10}\bar{V}_1 + \log_{10}\tau_{ij} + \log_{10}\bar{V}_2 \quad (2.63)$$

where $\log_{10}\bar{V}_1$ is the statistically-most-probable value of $\log_{10}V_1$ and similarly for $\log_{10}\bar{V}_2$. As discussed in ref. [25], equation (2.62) leads to quantum circuit rules. Furthermore provided the statistics of the virtual electrodes is independent of connectivity, equation (2.62) yields

$$\frac{\bar{\sigma}_{ij}}{\bar{\sigma}_{lm}} = \frac{\tau_{ij}}{\tau_{lm}} \quad (2.64)$$

This means that ratios of reported ‘statistically-most-probable conductances’ corresponding to different connectivities i,j and l,m are properties of the core of the molecule and the randomness associated with the unknown binding to electrodes disappears from the ratio.

2.9 M-theory

For simple PAH cores, to compute the quantities τ_{ij} a parameter-free theory of mid-gap electron transport (M-theory) was developed[1, 23], which describes the amplitude of the interference pattern on an arbitrary atomic orbital i due to an electron of energy E entering a core at orbital j . Each PAH is represented by a lattice of sites with nearest neighbour couplings and the Hamiltonian H is equated to a simple connectivity table C , whose entries C_{ij} were assigned a value -1 if sites i and j are nearest neighbours and a value of

zero otherwise. The M-functions $M_{ij}(E)$ are then given by i,j th elements of the matrix

$$M(E) = A(E)(E - C)^{-1} \quad (2.65)$$

where $A(E)$ is a scalar function of E , chosen for convenience such that for parental PAH cores, $M_{ij}(0)$ is an integer. For a given core, $A(E)$ does not affect conductance ratios, because $\tau_{ij}(E) = (M_{ij}(E))^2$ and therefore $A(E)$ cancels in equation (2.62) [23, 26].

Example of applying MRR

The starting point for applying MRR is to represent molecule by lattice of connected sites. For example, naphthalene lattice is represented as shown in Figure 2.11.

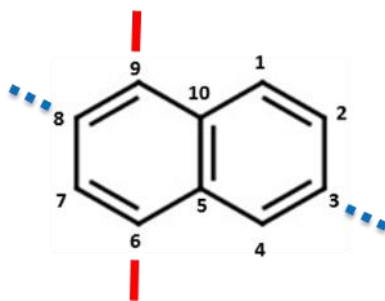


Figure 2.11: Molecular structure of naphthalene

The Hamiltonian H of naphthalene is equated to a simple connectivity table C , where the entries C_{ij} are assigned a value -1 if sites i and j are nearest neighbours and a value of zero otherwise. If E lies in the center of the H-L gap (i.e. $E = E_F = 0$), then for a bi-partite lattice described by a tight-binding model provides that all lattice sites are identical and the number of odd and even sites are equal, M-table can be obtained by inverting the H . The resulting M-table for naphthalene shown in Figure 1.1. As mentioned earlier, the MRR rule states that the ratio of conductances of two molecules is equal to the square of the ratio of their magic integers. So as expected from symmetry, M-table indicates that the conductances related to 6,7 and 8,9 connectivities are equal.

M_{ij}	2	4	6	8	10
1	-2	2	-1	1	-1
3	-1	-2	1	-1	1
5	1	-1	-1	1	-1
7	-1	1	-2	-1	1
9	1	-1	2	-2	-1

Table 1.1: M-table for naphthalene

Figure 2.10 shows naphthalene structure with two different connectivities 6,9 and 3,8. The magic integers related to these two connectivities are cycled in

matching colors with the connectivities as shown in Table. Calculating magic ratio for these two connectivities yields:

$$(M_{6,9}/M_{3,8})^2 = (2)^2/(-1)^2 = 4 \quad (2.66)$$

Which means that the conductance associated with contact site 6,9 is 4 times higher than the conductance associated with contact site 3,8. In the weak coupling limit, and when the Fermi energy of the electrodes lies in the centre of the HOMO-LUMO gap, the MRR is an exact formula for conductance ratios of tight-binding models of molecules, which is clear in tight binding representation in Figure 2.12. As expected from M-table, this Figure shows that the conductance related to 6,9 connectivity is higher than the conductance related to 3,8 connectivity by factor of 4.

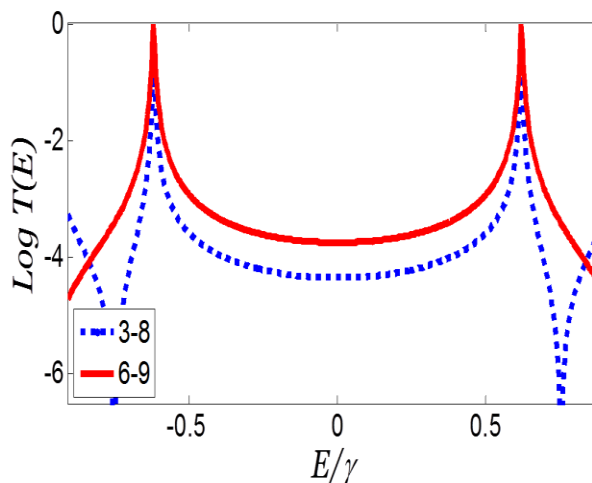


Figure 2.12: Tight binding result for the transmission coefficients of naphthalene: red and blue curves corresponds to 6,9 and 3,8 connectivities respectively.

Furthermore, DFT calculation shows similar trend as shown in Figure 2.13, where, as expected from M-table, the conductance associated with contact site 6,9 is higher than that related to contact site 3, 8.

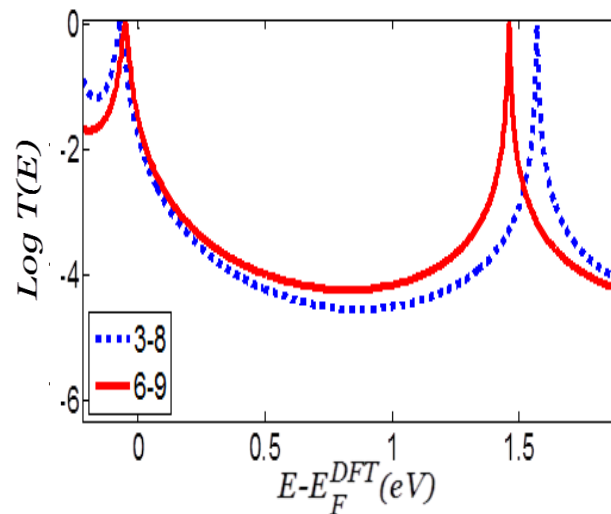


Figure 2.13: DFT result for the transmission coefficients of naphthalene: red and blue curves corresponds to 6,9 and 3,8 connectivities respectively.

2.10 Calculating binding energy using the counter poise method

Using the DFT approach to calculate the ground state geometry of different system configurations allows us to also calculate the binding energy between different parts of the system. However, these calculations are subject to

errors, due to the use of localized basis sets which are centered on the nuclei. If atoms are moved, then the basis set changes so any error arising from the incompleteness of the basis set will also change. One example of these errors is the overlapping basis sets of closed-shell atoms, where this generates synthetic short bond lengths combined with synthetic strong bonding energy which will give an inaccurate total energy of system. In the case of localized basis sets, as used in SIESTA, there is basis set superposition error (BSSE) presents and we have to correct for different basis sets of the two configurations [27]. In 1970, Boys and Bernardi proposed a technique to eliminate the BSSE in molecular complexes composed of two geometric configurations so-called the counterpoise correction [28]. The BSSE is obtained by recalculating using the mixed basis sets realised by introducing the ghost orbitals, and then subtracting the error from the uncorrected energy to calculate the binding energy E according to the following relation:

$$E_{binding} = E_{ab} - (E_a + E_b) \quad (2.67)$$

References

1. Geng, Y., et al., *Magic Ratios for Connectivity-Driven Electrical Conductance of Graphene-like Molecules*. Journal of the American Chemical Society, 2015. 137(13): p. 4469-4476.
2. Landauer, R., *Spatial variation of currents and fields due to localized scatterers in metallic conduction*. IBM Journal of Research and Development, 1957. 1(3): p. 223-231
3. Landauer, R., *Electrical transport in open and closed systems*, Z. Phys. B: Condens. Matter, vol. 68, no. 2-3, pp. 217–228, 1987.
4. Negele J W and Orland H *Quantum Many-Particle Systems* 1998 (New York Perseus Book Group)
5. Datta, S., *Electronic transport in mesoscopic systems*1997: Cambridge university press.
6. Büttiker, M., et al., *Generalized many-channel conductance formula with application to small rings*. Physical Review B, 1985. 31(10): p. 6207.
7. N. R. Claughton, M. Leadbeater, and C. J. Lambert, *Theory of Andreev Resonances in Quantum Dots*, Journal of Physics-Condensed Matter, vol. 7, no. 46, pp. 8757– 8784, 1995.
8. Economou, E.N., *Green's functions in quantum physics*1984: Springer.

9. Mello, P.A. and N.K. Kumar, *Quantum transport in mesoscopic systems: complexity and statistical fluctuations: a maximum-entropy viewpoint*. Vol. 4. 2004: Oxford University Press on Demand.
10. Breit, G. and E. Wigner, *Capture of slow neutrons*. Physical Review, 1936. **49**(7): p. 519.
11. Ke, S.-H., W. Yang, and H.U. Baranger, *Quantum-interference-controlled molecular electronics*. Nano letters, 2008. **8**(10): p. 3257-3261.
12. Stadler, R., *Quantum interference effects in electron transport through nitrobenzene with pyridil anchor groups*. Physical Review B, 2009. **80**(12): p. 125401.
13. Fano, U., *Effects of configuration interaction on intensities and phase shifts*. Physical Review, 1961. **124**(6): p. 1866.
14. Papadopoulos, T., I. Grace, and C. Lambert, *Control of electron transport through Fano resonances in molecular wires*. Physical Review B, 2006. **74**(19): p. 193306.
15. Sedghi, G., et al., Long-range electron tunnelling in oligo-porphyrin molecular wires. Nat Nanotechnol, 2011. 6(8): p. 517-23.
16. Zhao, X., et al., *Oligo(aryleneethynylene)s with Terminal Pyridyl Groups: Synthesis and Length Dependence of the Tunneling-to-Hopping Transition*

- of Single-Molecule Conductances*. Chemistry of Materials, 2013. **25**(21): p. 4340-4347.
17. Magoga, M. and C. Joachim, *Conductance of molecular wires connected or bonded in parallel*. Physical Review B, 1999. **59**(24): p. 16011-16021.
 18. Mol, J.A., et al., *Graphene-porphyrin single-molecule transistors*. Nanoscale, 2015. **7**(31): p. 13181-5.
 19. Hong, W., et al., *An MCBJ case study: The influence of pi-conjugation on the single-molecule conductance at a solid/liquid interface*. Beilstein J Nanotechnol, 2011. **2**: p. 699-713.
 20. Prins, F., et al., *Room-temperature gating of molecular junctions using few-layer graphene nanogap electrodes*. Nano Lett, 2011. **11**(11): p. 4607-11
 21. Xia, J., et al., *Breakdown of Interference Rules in Azulene, a Nonalternant Hydrocarbon*. Nano Letters, 2014. **14**(5): p. 2941-2945.

6389.
 22. Markussen, T., R. Stadler, and K.S. Thygesen, *The Relation between Structure and Quantum Interference in Single Molecule Junctions*. Nano Letters, 2010. **10**(10): p. 4260-4265.

23. Sangtarash, S., et al., *Searching the Hearts of Graphene-like Molecules for Simplicity, Sensitivity, and Logic*. Journal of the American Chemical Society, 2015. **137**(35): p. 11425-11431.
24. Lambert, C.J., Basic concepts of quantum interference and electron transport in single-molecule electronics. Chem Soc Rev, 2015. 44(4): p. 875-88.
25. Manrique, D.Z., et al., *A quantum circuit rule for interference effects in single-molecule electrical junctions*. Nat Commun, 2015. **6**: p.
26. Sangtarash, S., H. Sadeghi, and C.J. Lambert, *Exploring quantum interference in heteroatom-substituted graphene-like molecules*. Nanoscale, 2016. 8(27): p. 13199-13205.
27. Visontai, D., I. Grace, and C. Lambert, *Electron transport through ribbonlike molecular wires calculated using density-functional theory and Green's function formalism*. Physical review b, 2010. **81**(3): p. 035409.
28. Milani, A., et al., *Charge Transfer and Vibrational Structure of sp-Hybridized Carbon Atomic Wires Probed by Surface Enhanced Raman Spectroscopy*. The Journal of Physical Chemistry C, 2011. **115**(26): p. 12836-12843.

Chapter 3

Heteroatom Induced Molecular Asymmetry Tunes Quantum Interference in Charge Transport through Single-molecule Junctions with Five-membered Rings.

The following study is a collaborative work between myself, Prof. Martin and Prof. Wenjing (Durham and Xiamen Universities).

3.1 Introduction

Quantum interference (QI) effects have recently attracted great interest in studies of the charge transport at the single-molecule scale [1,2,3,4,5,6]. As determined by the phases of the partial de Broglie waves traversing different paths [7,8,9], QI provides a unique way to tune the single-molecule conductance by orders of magnitude without incorporating substituent groups, extending molecular length or changing the surrounding environment of the molecule. To date most reports of QI in cyclic molecules have been

restricted to compounds with central six-membered rings [10,11,12,13,14]. Although it has not been observed experimentally, QI in central five-membered rings is suggested to be a promising way to vary the molecular topology and increase structural diversity of single-molecule devices [15].

The incorporation of heteroatoms into a central di-functionalized five-membered-system leads to the structural asymmetry of the molecular junctions [15]. Recent studies suggest that an asymmetric pyridine modifies the pattern of QI within the core of the molecular backbone and promotes charge transport through single-molecule junctions [16]. Therefore, five-membered heterocyclics provide a natural platform to investigate the interplay of QI effects and structural asymmetry of the core unit in charge transport through single-molecule junctions.

3.2 Discussion and results

Here I study the single-molecule conductances of a series of eight compounds of the type X-Y-X as shown in Figure 3.1, where X is a pyridyl anchor and Y is a five-membered core ring, furan (**1**, **5**), pyrrole (**2**, **6**), thiophene (**3**, **7**) or cyclopentadiene cores (**4**, **8**). There are three notable features in their molecular design: (i) all of the molecules have terminal pyridyl anchoring units (X) at both ends; (ii) each molecule has one of four

different 5-membered core units (Y), and (iii) the core is either symmetrically substituted (i.e. 2,5-difunctionalized; **1-4**) or asymmetrically substituted (i.e. 2,4-difunctionalized; **5-8**). These compounds provide a unique opportunity to investigate two issues. First, whether the QI effect is general for other conjugated systems, besides those previously studied with aromatic six-membered central rings [10,11,12,13,14]. Second, what is the interplay between QI and structural asymmetry in charge transport through five-membered core units?

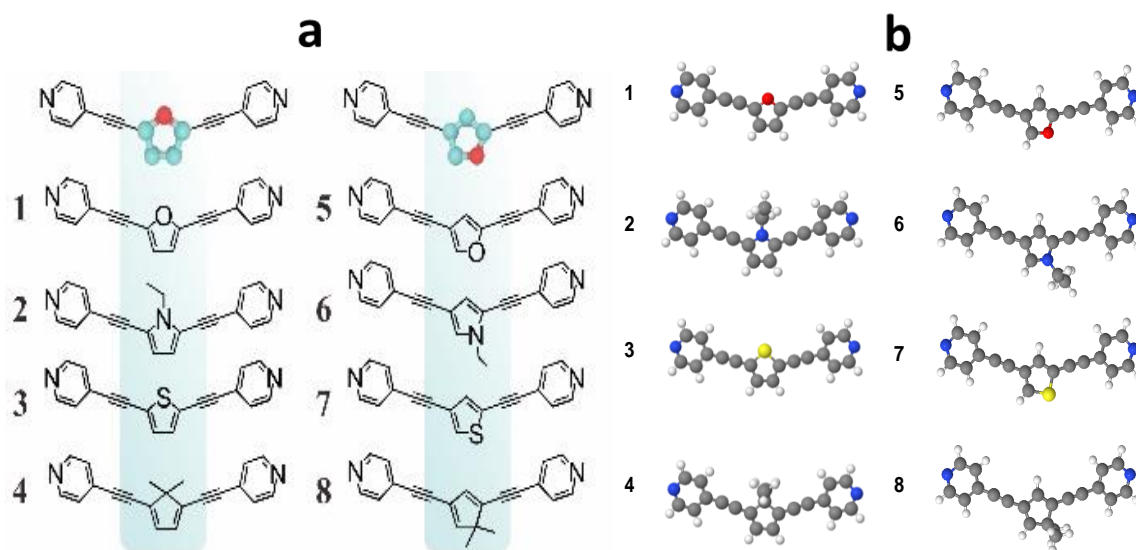
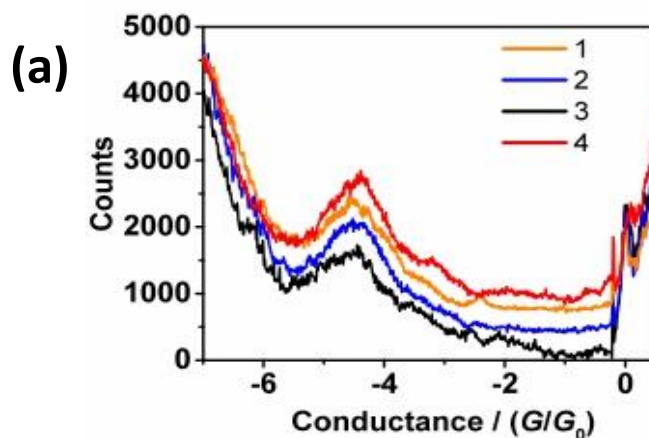


Figure 3.1: The molecules: **1-4** the symmetric compounds and **5-8** the asymmetric compounds. (a) the schematic of MCBJ and (b) the relaxed structures.

In Xiamen University, the mechanically controllable break junction (MCBJ) technique was used to measure the single-molecule conductances of

compounds **1-8** where the experiments were carried out in ambient conditions at room temperature. Figure 3.2a and 3.2b present the conductance histograms of **1-4** and **5-8** compounds respectively, from which the discernible peaks are centered at the very similar values of $10^{-4.54 \pm 0.37} G_0$, $10^{-4.57 \pm 1.08} G_0$, $10^{-4.63 \pm 0.35} G_0$, and $10^{-4.49 \pm 0.60} G_0$ for compounds **1-4**, respectively. In contrast, the single-molecule conductance values of **5-8** are consistently lower than that of the series **1-4**, giving the direct evidence of destructive QI. For compound **7** there is no peak in the conductance histogram, implying that the single-molecule conductance is out of the measuring range i.e., it is lower than $10^{-6} G_0$. Based on that, Table 3.1 summarizes the single-molecule conductances and the lengths of compounds **1-8** obtained from MCBJ measurements.



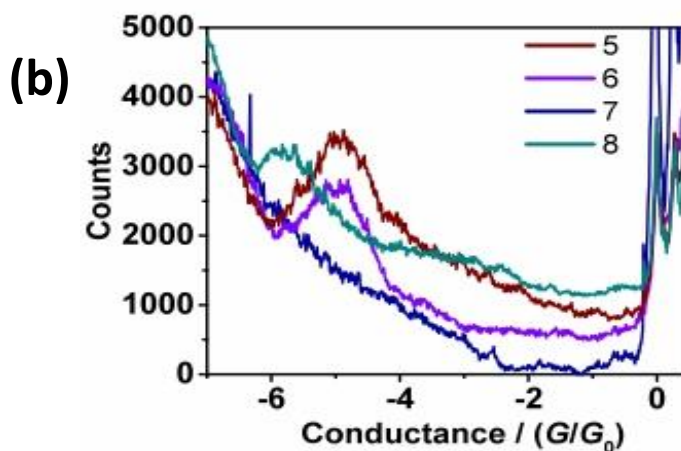


Figure 3.2 : One-dimensional conductance histograms for compounds: (a) **1-4** and (b) **5-8**

Compounds	Measured Conductance / $\log(G/G_0)$	Measured Length / nm
1	-4.54 ± 0.37	1.39 ± 0.15
2	-4.57 ± 0.54	1.38 ± 0.18
3	-4.63 ± 0.36	1.36 ± 0.16
4	-4.49 ± 0.60	1.38 ± 0.13
5	-4.94 ± 0.40	1.44 ± 0.26
6	-5.03 ± 0.35	1.47 ± 0.23
7	<-6	/
8	-5.85 ± 0.34	1.40 ± 0.16

Table 3.1. Single-molecule conductances and lengths extracted from MCBJ measurements.

The data show that for the symmetric compounds **1-4** there is no statistical variation of conductance with the bridging atom (S, N, O or C). It is instructive to compare these results with the work of Chen et al on a series of compounds having similar structures to **1**, **3**, and **4**, except that they were wired to gold electrodes by amino anchors,[17] rather than pyridyl as studied here. Amino and pyridyl anchors lead to HOMO- and LUMO-dominated conductance, respectively. For the amino anchors the clear trend in conductance was cyclopentadiene > furan > thiophene. This led to the conclusion that “aromaticity decreases single-molecule junction conductance”[17]. Where this study indicates that for the symmetrical compounds **1-4** the pyridyl anchor dominates the conductance, and there is no statistically-significant dependence on the aromaticity of the core. It is also noticed that the single-molecule conductances of the pyridyl compounds are consistently lower than for the amino anchored analogs due to the different anchoring groups [9-10].

For compounds **5-8**, the electronegativity decreases in the sequence O (3.44) > N (3.04) > S (2.58) \approx C (2.55) from the periodic table of electronegativity by the Pauling scale, thus for the studied compounds, the degree of asymmetry decreases in the sequence **5** > **6** > **7** \approx **8**. As listed in Table 1, the

lowest conductance values are obtained for **7** and **8**, where the heteroatoms have the lowest electronegativities, suggesting a strong correlation between the molecular asymmetry, electronegativity and single-molecule conductance.

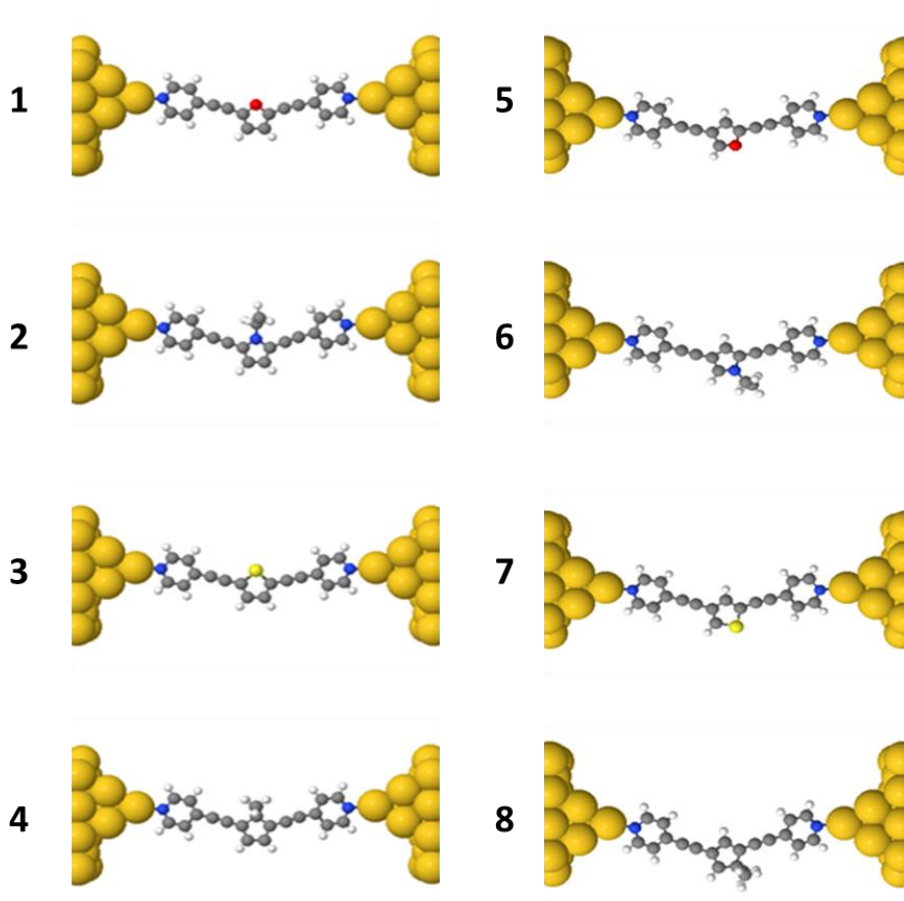


Figure 3.3: Relaxed structures of the symmetric (**1-4**) and asymmetric (**5-8**) compounds placed between electrodes, when the electrodes are connected to the nitrogen atoms of the pyridyl anchoring groups.

To investigate the interplay between structural asymmetry and QI in molecules wired between two electrodes, I firstly relaxed the compounds shown in Figure 3.1 individually using the SIESTA code [18]. Next the relaxed compounds were placed between two gold electrodes. These structures were again geometrically relaxed with SIESTA to obtain optimal junction geometries as shown in Figure 3.3. Then the transmission coefficients $T(E)$ of electrons with energy E passing from one electrode to another through molecules were calculated using the GOLLUM transport code [19] (see methods).

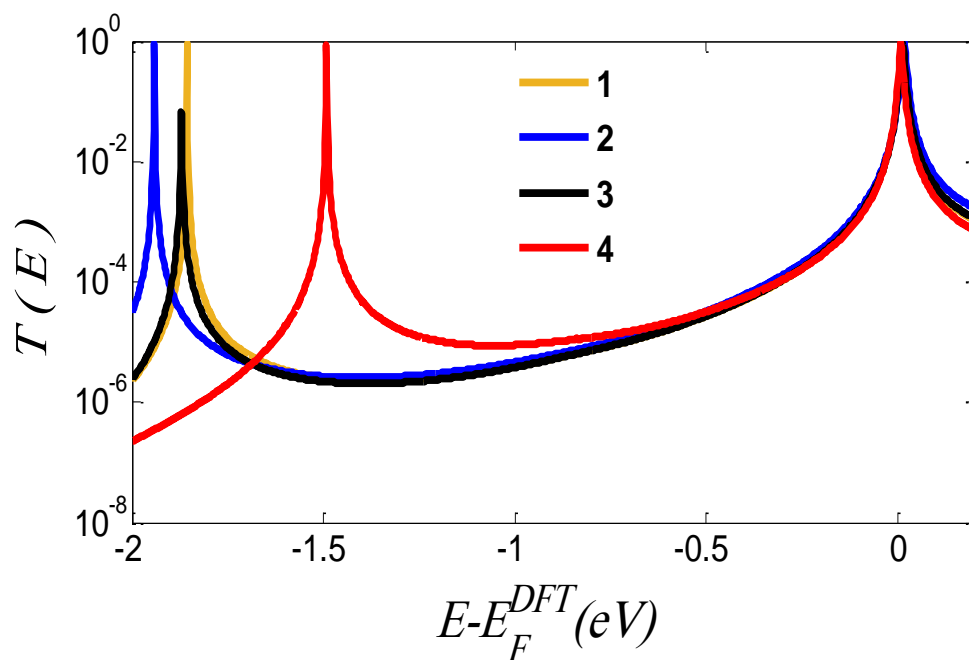


Figure 3.4: DFT results of the transmission coefficients of the symmetric compounds 1-4.

Figure 3.4 and 3.5 show the calculated $T(E)$ of compounds **1-8**. For the symmetric compounds, Figure 3.4, it is found that the $T(E)$ values of **1-4** in the LUMO dominated regime $-0.5 \text{ eV} < E < 0$ are quite similar. Since charge transport through pyridine terminated molecules takes place in the tail of the LUMO, the calculations are in good agreement with the experimental findings.

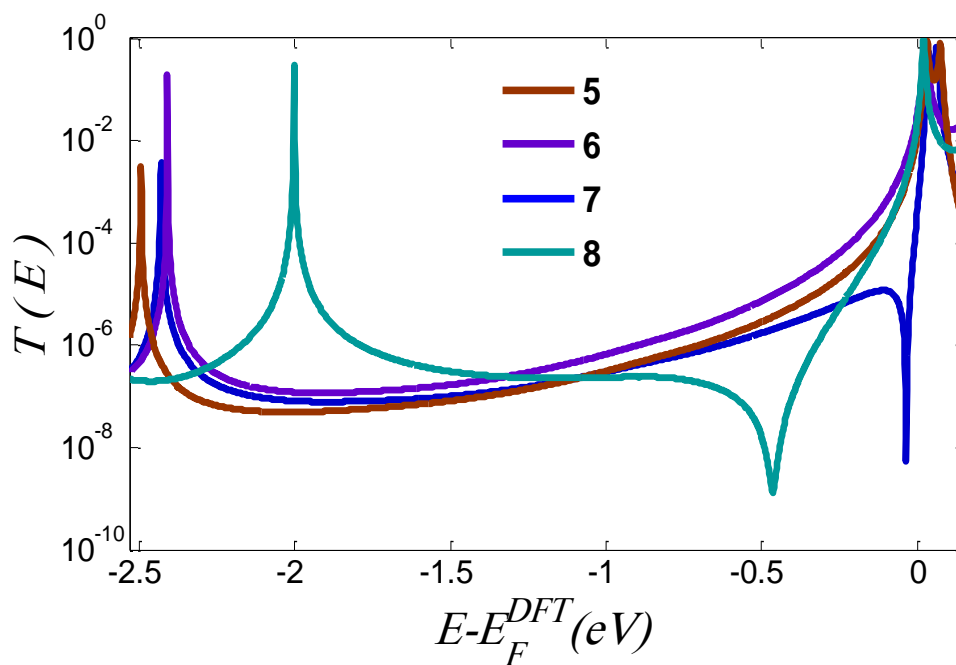


Figure 3.5: DFT results of the transmission coefficients of the asymmetric compounds **5-8**

As shown in Figure 3.5, the calculated $T(E)$ of **5-8** is significantly lower than that of **1-4**. Furthermore, for compounds **7** and **8**, sharp drops in the

transmission curve, i.e., the anti-resonance features, are observed in the tail of the LUMO peaks. The presence of these anti-resonances correlates with the lower measured conductances for these compounds. In contrast, for **5** and **6**, as shown in Figure 3.5, there are no anti-resonances within the HOMO-LUMO gap, which correlates with the higher conductances that measured experimentally. The absence of anti-resonance features within the HOMO-LUMO gap suggests that the high electronic asymmetry of the core unit, which originates from the greater electronegativities of the heteroatoms, moves the anti-resonance features out of the HOMO-LUMO gap of the molecular junction, and thus QI has a minor effect on the charge transport through single-molecule junctions. These theoretical results and our experimental findings suggest that molecular asymmetry affords a novel approach to tuning destructive QI and charge transport through single-molecule junctions.

To summarize, I investigated the synergistic effect of molecular symmetry and QI on the charge transport through single-molecule junctions with five-membered core rings. It was found that for the symmetric 2,5-disubstituted series **1-4**, the pyridyl anchors dominate the conductance and there is no statistically significant variation with core unit. In contrast, the conductances

of the asymmetric 2,4-disubstituted series **5-8** are significantly lower than those of the symmetric **1-4** series, reflecting the presence of destructive QI. More importantly, the control of molecular asymmetry via the heteroatoms provides the tuning of destructive QI in the charge transport through single-molecule junctions. DFT calculations reveal that for asymmetric molecules, the electronegativity of the heteroatoms can be used to move anti-resonance features into or out of the HOMO-LUMO gap, which controls the destructive QI effect. This work establishes a route for the design of building blocks through incorporating heteroatoms into molecular structure, and further demonstrates a novel yet simple strategy for tuning QI in single-molecule electronics via asymmetry. This has promising applications in the design of future molecular-electronic components.

To gain more insight in the relation between QI and structural asymmetry in charge transport through five-membered core units, further theoretical calculations have been carried out. Within the same theoretical framework, I calculated the transmission coefficients of the same cores with different anchor groups, using SIESTA code combined with quantum transport code GOLLUM, where the pyridyl anchors were replaced with thiol anchoring

groups. Figure 3.6 represents the new eight compounds placed between two gold electrodes **9-16** after relaxation.

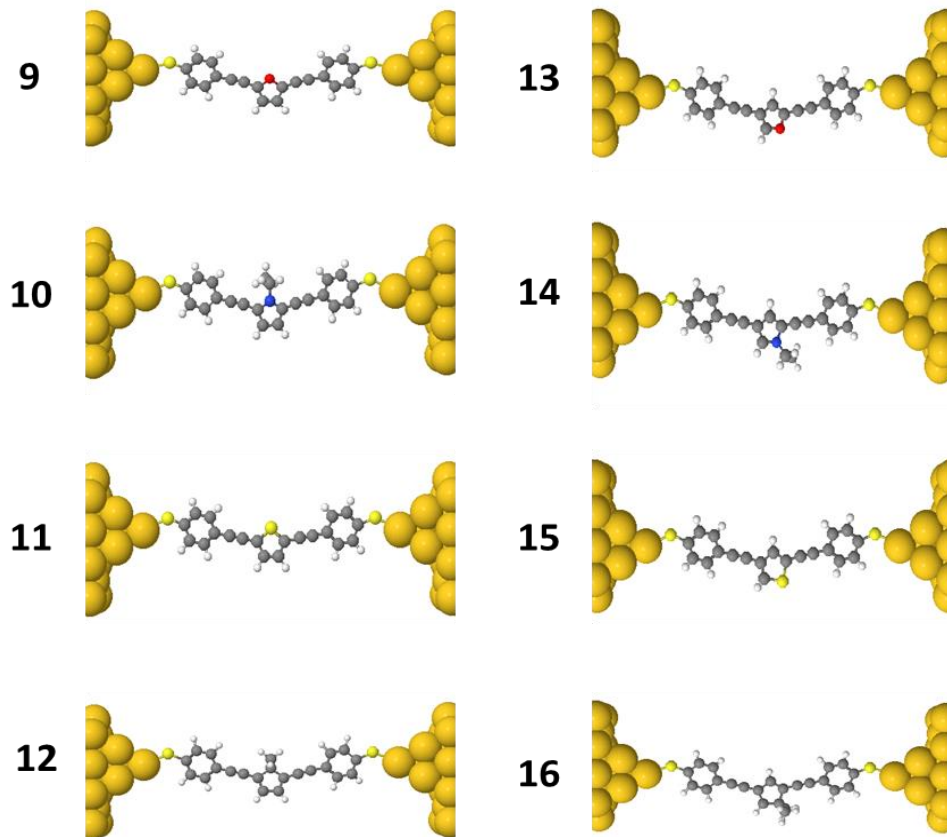


Figure 3.6: Relaxed structures of the symmetric (**9-12**) and asymmetric (**13-16**) compounds placed between electrodes, when the electrodes are connected to the sulfur atoms of the thiol anchoring groups.

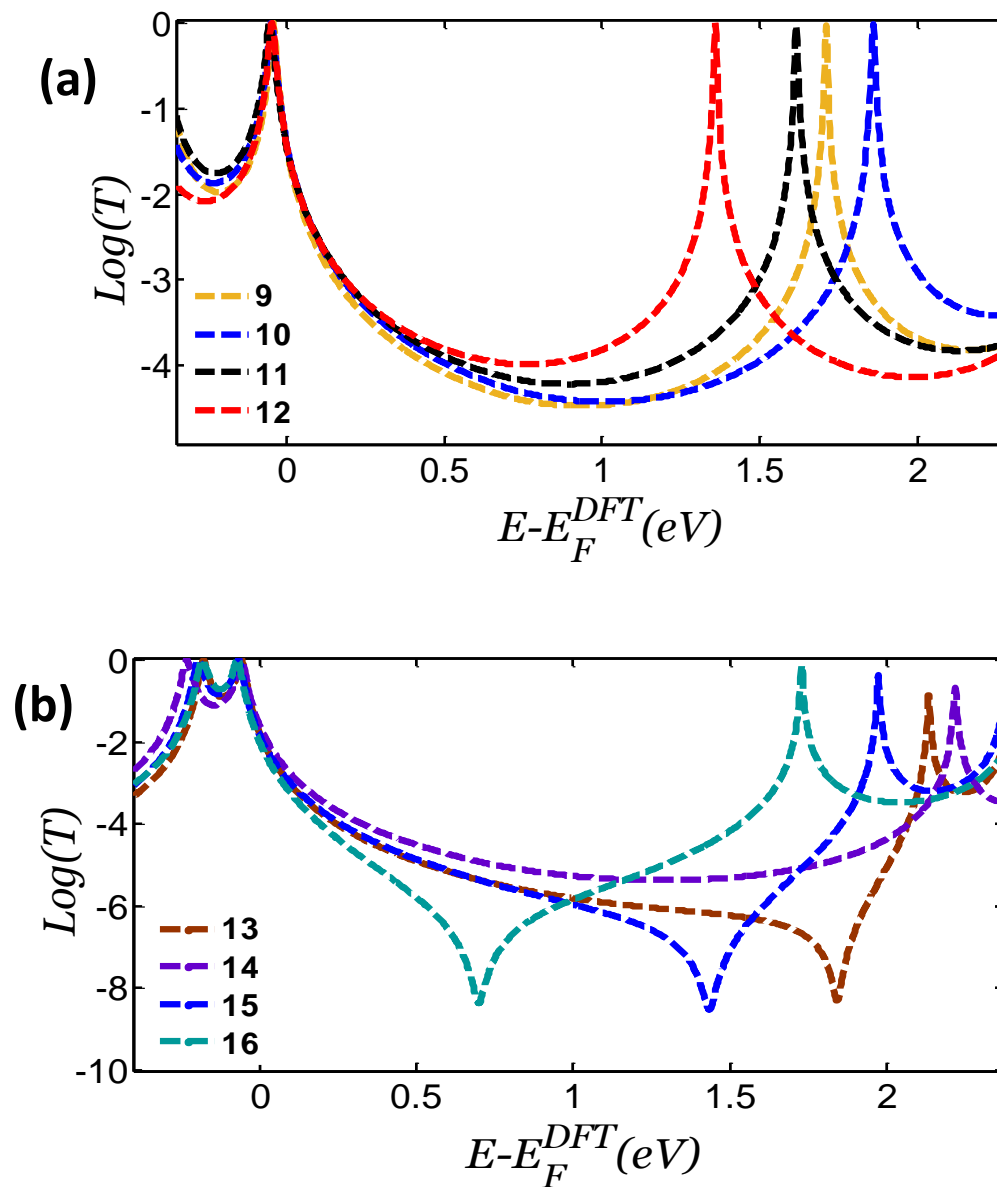


Figure 3.7: DFT results of the transmission coefficients for (a) compounds **9-12** and (b) compounds **13-16**

For the symmetric series **9-12**, Figure 3.7a shows that the $T(E)$ values in small HOMO dominated regime are quite similar, therefore, there is no

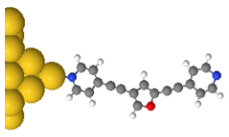
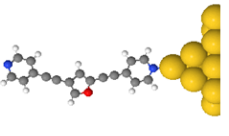
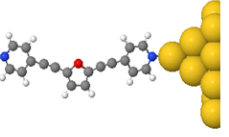
significant variation in the $T(E)$ with the core unit over this range of energy. After that $T(E)$ starts to vary gradually and follow the sequence: **12** (cyclopentadiene) > **11** (thiophene) > **10** (pyrrole) > **9** (furan) within wide range of energy which differs from previous result (with pyridyl anchor). Clearly, a comparison between the results obtained using these two different anchors depends on the position of the Fermi energy. However, in general, the DFT results of **9-12** compounds are similar to those of the **1-4** compounds over a small range of energy confirming the impact of the anchoring groups on the charge transport through the molecule. Figure 3.7b shows that $T(E)$ of the asymmetric compounds **13-16** are remarkably lower than those of **9-12** which confirms the presence of the destructive interference. Moreover, sharp anti-resonances are observed in the transmission curves of compounds **13, 15** and **16** within the HOMO-LUMO gap as a feature of destructive interference.

Comparing figures 3.4 and 3.7a reveals that the calculated $T(E)$ of the symmetric **9-12** compounds with thiol anchoring groups are in general higher than those of **1-4** compounds with pyridyl anchoring group. Similarly, for the asymmetric compounds, Figure 3.7b shows that the compounds **13-16** with

thiol linker have $T(E)$ slightly higher than that of **5-8** with pyridyl linker in Figure 3.5.

Further insight into **1-8** compounds can be obtained by studying the relation between the binding energy E^b and the symmetric and asymmetric structure. To do so, I carried out DFT based calculations of the molecular binding energies using counterpoise method for these compounds in presence of one lead using two different basis sets: double-zeta plus polarization (DZP) and single zeta (SZ). The resulting binding energies for **1-8** compounds are summarized in Tables 3.2 and 3.3 [20, 21].

(a)

Structure	DZP	SZ
	-0.07	-1.36
	-0.11	-1.43
	-0.21	-1.76

(b)

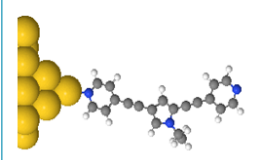
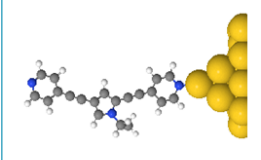
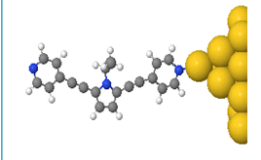
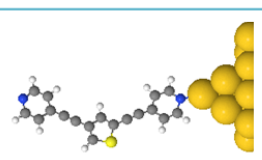
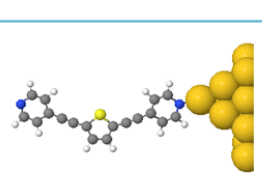
Structure	DZP	SZ
	-0.07	-1.22
	-0.08	-1.27
	-0.13	-1.54

Table 3.2: The binding energies (in eV) in presence of one lead, the top two rows and the bottom row in tables (a, b) correspond to the asymmetric compounds **5**, **6** and symmetric compounds **1**, **2**, respectively.

(c)

Structure	DZP	SZ
	-0.06	-1.32
	-0.12	-1.42
	-0.22	-1.78

(d)

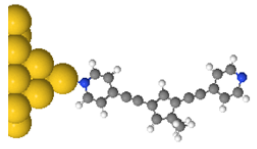
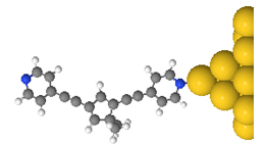
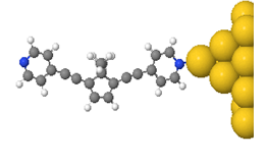
Structure	DZP	SZ
	-0.14	-1.5
	-0.18	-1.6
	-0.31	-1.9

Table 3.3: The binding energies (in eV) in presence of one lead, the top two rows and the bottom row in tables (c, d) correspond to the asymmetric compounds **7, 8** and symmetric compounds **3, 4**, respectively.

Tables 3.2 and 3.3 show a comparison between the binding energies of the compounds **1-8**. Comparing the binding energies of the symmetric compounds **1-4** and of the asymmetric compounds **5-8** separately reveals that there is no significant difference in their binding energies. In contrast, the binding energies of the symmetric compounds are slightly higher than those of the asymmetric compounds through each compound in both cases (DZP, SZ). Furthermore, the binding energies calculated using the SZ basis set are

higher than the binding energies resulting from using DZP basis set through all compounds.

3.3 Conclusion

In this chapter, the single-molecule conductances of eight compounds with five-membered ring core units (**1-8**) have been studied experimentally and theoretically. The results show that for the series **1-4** there is no remarkable variation in the conductances with the core unit, whereas the conductances of the asymmetric series **5-8** are significantly low compared to those of the symmetric series which reflects the presence of the destructive QI. Further theoretical study has been done using thiol linkers instead of pyridyl linkers (in the **1-8** compounds). Using thiol anchoring groups gives **9-16** compounds. The DFT results of **9-16** compounds defer from that of **1-8** compounds confirming the impact of the anchoring groups on the charge transport through the molecule. Moreover, the binding energies of compounds **1-8** have been calculated and the results indicate that: for asymmetric compounds the binding energy values when the heteroatom are close to the lead are slightly higher than the binding energy values when the heteroatom far from the lead. Moreover, the binding energies of the symmetric series slightly

higher than those of the asymmetric series revealing that there is no strong effect of the molecular asymmetry on the binding energies of **1-8** compounds.

3.4 Calculations methods

DFT calculations: The optimized geometry and ground state Hamiltonian and overlap matrix elements of each structure was self-consistently obtained using the SIESTA [14] implementation of density functional theory (DFT). SIESTA employs norm-conserving pseudo-potentials to account for the core electrons and linear combinations of atomic orbitals to construct the valence states. The generalized gradient approximation (GGA) of the exchange and correlation functional is used with the Perdew-Burke-Ernzerhof parameterization (PBE) a double- ζ polarized (DZP) basis set, a real-space grid defined with an equivalent energy cut-off of 250 Ry. The geometry optimization for each structure is performed to the forces smaller than 10 meV/Ang.

Transport calculations: The mean-field Hamiltonian obtained from the converged DFT calculation or a tight-binding Hamiltonian (using single orbital energy site per atom with Hückel parameterisation) was combined with implementation non-equilibrium Green's function method, GOLLUM [15], to calculate the phase-coherent, elastic scattering properties of the each

system consisting of left gold (source) and right gold (drain) leads and the scattering region (molecule). The transmission coefficient $T(E)$ for electrons of energy E (passing from the source to the drain) is calculated via the relation: $T(E) = \text{Trace}(\Gamma_R(E)G^R(E)\Gamma_L(E)G^{R\dagger}(E))$. In this expression, $\Gamma_{L,R}(E) = i(\Sigma_{L,R}(E) - \Sigma_{L,R}^\dagger(E))$ describe the level broadening due to the coupling between left (L) and right (R) electrodes and the central scattering region, $\Sigma_{L,R}(E)$ are the retarded self-energies associated with this coupling and $G^R = (ES - H - \Sigma_L - \Sigma_R)^{-1}$ is the retarded Green's function, where H is the Hamiltonian and S is overlap matrix. Using obtained transmission coefficient $T(E)$, the conductance could be calculated by Landauer formula ($G = G_0 \int dE T(E)(-\partial f/\partial E)$) where $G_0 = 2e^2/h$ is conductance quantum.

References

1. Baer, R. and D. Neuhauser, Phase coherent electronics: A molecular switch based on quantum interference. *Journal of the American Chemical Society*, 2002. 124(16): p. 4200-4201.
2. Cardamone, D.M., C.A. Stafford, and S. Mazumdar, Controlling Quantum Transport through a Single Molecule. *Nano Letters*, 2006. 6(11): p. 2422-2426.
3. Guedon, C.M., et al., Observation of quantum interference in molecular charge transport. *Nat Nanotechnol*, 2012. 7(5): p. 305-9.
4. Valkenier, H., et al., Cross-conjugation and quantum interference: a general correlation? *Physical Chemistry Chemical Physics*, 2014. 16(2): p. 653-662.
5. Lambert, C.J., Basic concepts of quantum interference and electron transport in single-molecule electronics. *Chem Soc Rev*, 2015. 44(4): p. 875-88.
6. Su, T.A., et al., Chemical principles of single-molecule electronics. *Nature Reviews Materials*, 2016. 1(3): p. 15.

7. Geng, Y., et al., Magic Ratios for Connectivity-Driven Electrical Conductance of Graphene-like Molecules. *Journal of the American Chemical Society*, 2015. 137(13): p. 4469-4476.
8. Sangtarash, S., et al., Searching the Hearts of Graphene-like Molecules for Simplicity, Sensitivity, and Logic. *Journal of the American Chemical Society*, 2015. 137(35): p. 11425-11431.
9. Sangtarash, S., H. Sadeghi, and C.J. Lambert, Exploring quantum interference in heteroatom-substituted graphene-like molecules. *Nanoscale*, 2016. 8(27): p. 13199-13205.
10. Arroyo, C.R., et al., Quantum interference effects at room temperature in OPV-based single-molecule junctions. *Nanoscale Research Letters*, 2013. 8: p. 1-6.
11. Arroyo, C.R., et al., Signatures of Quantum Interference Effects on Charge Transport Through a Single Benzene Ring. *Angewandte Chemie-International Edition*, 2013. 52(11): p. 3152-3155.
12. Garner, M.H., G.C. Solomon, and M. Strange, Tuning Conductance in Aromatic Molecules: Constructive and Counteractive Substituent Effects. *Journal of Physical Chemistry C*, 2016. 120(17): p. 9097-9103.

13. Manrique, D.Z., et al., A quantum circuit rule for interference effects in single-molecule electrical junctions. *Nature Communications*, 2015. 6.
14. Solomon, G.C., et al., Exploring local currents in molecular junctions. *Nature Chemistry*, 2010. 2(3): p. 223-228.
15. Borges, A. and G.C. Solomon, Effects of Aromaticity and Connectivity on the Conductance of Five-Membered Rings. *Journal of Physical Chemistry C*, 2017. 121(15): p. 8272-8279.
16. Liu, X.S., et al., Gating of Quantum Interference in Molecular Junctions by Heteroatom Substitution. *Angewandte Chemie-International Edition*, 2017. 56(1): p. 173-176.
17. Chen, W., et al., Aromaticity Decreases Single-Molecule Junction Conductance. *Journal of the American Chemical Society*, 2014. **136**(3): p. 918-920.
18. Ferrer, J., et al., GOLLUM: a next-generation simulation tool for electron, thermal and spin transport. *New Journal of Physics*, 2014. 16(9): p. 093029.
19. José, M.S., et al., The SIESTA method for ab initio order- N materials simulation. *Journal of Physics: Condensed Matter*, 2002. 14(11): p. 2745.

20. Jansen, H. & Ros, P. Non-empirical molecular orbital calculations on the protonation of carbon monoxide. *Chemical Physics Letters* 3, 140-143 (1969).

21. Boys, S. F. & Bernardi, F. d. The calculation of small molecular interactions by the differences of separate total energies. Some procedures with reduced errors. *Molecular Physics* 19, 553-566 (1970).

Chapter 4

Conductance of Antiaromatic Graphene-like Structures with Different Connectivities

This study is a collaborative work between (Lancaster, Durham and Xiamen Universities) and the experiments are in progress.

4.1 Introduction

Polycyclic aromatic hydrocarbons (PAHs) have received significant interest in recent years in many different fields[1, 2], due to their unique electronic properties and their role in the design and development of molecular electronic devices[3]. Since PAHs are well-defined and defect free, they also have a potential to be used as models for understanding transport in graphene, considered an infinite alternant PAH, and graphene-based nanostructures[4]. According to the Huckel aromaticity rules [5], polycyclic hydrocarbons are described as aromatic compounds when they are

cyclic, planar and have $4n+2$ π -electrons. If they, instead, possess $4n$ π -electrons then they are classified as antiaromatic components and would analogously be called polycyclic antiaromatic hydrocarbons (PAAH) [6].

In general the antiaromaticity definition is somewhat debatable, however the concept has attracted a great interest due to unusual features of the antiaromatic compounds such as instability, high reactivity, smaller gap (compared to aromatic compounds) and magnetic properties [7, 8]. Consequently, antiaromatic molecules have been predicted to have remarkable conducting properties [8]. However, reports about antiaromatic molecules are rare [6] due to their instability and difficult synthesis.

4.2 Discussion and results

Over the years, a large variety of experimental techniques and theoretical methods have been employed to explore the quantum transport mechanisms and elucidate the conditions for the appearance of constructive or destructive interference [9, 10]. In the simplest realization of the single molecular junction, where electrons are injected at the Fermi energy E_F of the electrodes, the constructive quantum interference appears when E_F coincides with a delocalized energy level E_n of the molecule. Within the same

conceptual framework, destructive quantum interference arises when E_F coincides with the energy E_b of a bound state [9, 11]. Practically, the molecules located in a junction usually do not experience these types of quantum interference except if the energy levels are tuned by electrostatic, electrochemical or mechanical gating, because E_F is usually located in the HOMO-LUMO gap. Therefore, most of discussions have concentrated on exploring destructive or constructive quantum interference when E_F lies in the middle of the HOMO-LUMO gap [12, 13] resulting in some fundamental theories .

One new and efficient approach, (discussed in section (2.8)), is a recent mid gap transport theory, which provides a simple rule called magic ratio rule "MRR" to determine the non-zero values of electrical conductance arising from constructive quantum interference in aromatic molecules [12, 13]. The aim of the present work is to examine the validity of the "MRR" for antiaromatic molecules by investigating the single molecule transport properties of tris-(benzocyclobutadieno)triphenylene [14], shown in Figure 4.1 , for different connectivities to gold electrodes using two different linker groups. Tris(benzocyclobutadieno)triphenylene is a polycyclic hydrocarbons antiaromatic molecule consisting of six- and four-membered rings. Each

four-membered ring is in contact with two six-membered rings. It can also be viewed as a conjunction of three biphenylene molecules attached to cross conjugated core (benzene) which results in C_3 -symmetry compound [14]. These kinds of compounds have drawn remarkable attention due to their potential as molecular magnetic and conducting materials [14, 15]. Furthermore, tris(benzocyclobutadieno)-triphenylene is a relatively large molecule and contains a combination of aromatic and antiaromatic rings [12]. It is thus interesting to investigate how MRR works for such antiaromatic molecule.

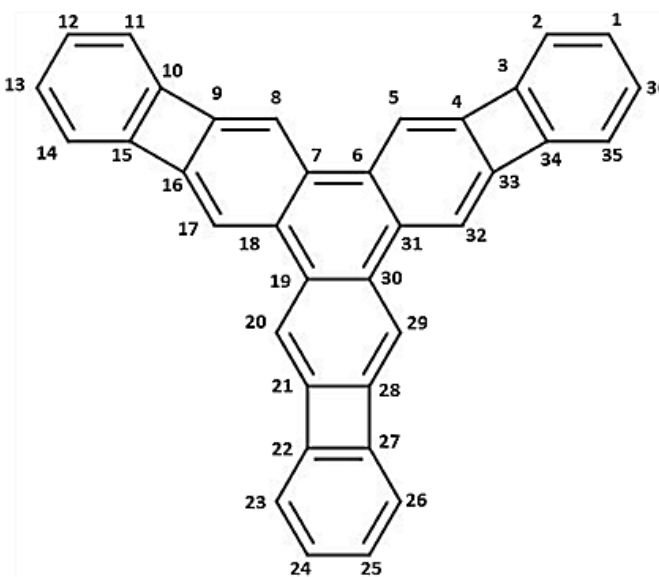


Figure 4.1: Molecular structures of tris(benzocyclobutadieno)triphenylene.

According to the MRR , the M-table for this molecule is 18×18 matrix and contains all the allowed nonzero values of M_{ij} when i is odd and j is even (or vice versa), as shown in Table 4.1 (Note that for such a bipartite molecule M_{ij} vanishes when i, j are both odd or both even). As a simple test to examine MRR validity, let us consider (11- 12) and (13- 14) connectivities. As expected from symmetry, Table 4.1 predicts that the mid-gap transmission coefficients associated with these contact sites to be equal.

M_{ij}	2	4	6	8	10	12	14	16	18	20	22	24	26	28	30	32	34	36
1	-13	-9	9	-3	-3	3	-3	6	-6	2	2	-2	2	-4	4	-13	22	-22
3	-22	9	-9	3	3	-3	3	-6	6	-2	-2	2	-2	4	-4	13	-22	22
5	13	-26	-9	3	3	-3	3	-6	6	-2	-2	2	-2	4	-4	13	13	-13
7	-4	8	-8	-9	-9	9	-9	18	-18	6	6	-6	6	-12	12	-4	-4	4
9	4	-8	8	-26	9	-9	9	-18	18	-6	-6	6	-6	12	-12	4	4	-4
11	-2	4	-4	13	-22	-13	13	9	-9	3	3	-3	3	-6	6	-2	-2	2
13	2	-4	4	-13	22	-22	-13	-9	9	-3	-3	3	-3	6	-6	2	2	-2
15	-2	4	-4	13	-22	22	-22	9	-9	3	3	-3	3	-6	6	-2	-2	2
17	-2	4	-4	13	13	-13	13	-26	-9	3	3	-3	3	-6	6	-2	-2	2
19	6	-12	12	-4	-4	4	-4	8	-8	-9	-9	9	-9	18	-18	6	6	-6
21	-6	12	-12	4	4	-4	4	-8	8	-26	9	-9	9	-18	18	-6	-6	6
23	3	-6	6	-2	-2	2	-2	4	-4	13	-22	-13	13	9	-9	3	3	-3
25	-3	6	-6	2	2	-2	2	-4	4	-13	22	-22	-13	-9	9	-3	-3	3
27	3	-6	6	-2	-2	2	-2	4	-4	13	-22	22	-22	9	-9	3	3	-3
29	3	-6	6	-2	-2	2	-2	4	-4	13	13	-13	13	-26	-9	3	3	-3
31	-9	18	-18	6	6	-6	6	-12	12	-4	-4	4	-4	8	-8	-9	-9	9
33	9	-18	18	-6	-6	6	-6	12	-12	4	4	-4	4	-8	8	-26	9	-9
35	13	9	-9	3	3	-3	3	-6	6	-2	-2	2	-2	4	-4	13	-22	-13

Table 4.1: M-Table of tris(benzocyclobutadieno)triphenylene.

Based on M-table, shown in Figure 4.1, I compared the transmission coefficients of tris(benzocyclobutadieno)triphenylene for three different connectivities. MRR predicts that the transmission coefficients of tris(benzocyclobutadieno)triphenylene with contact sites (1-12) and (1-14) are equal and these transmission coefficients in turn higher than the transmission coefficient associated with contact site (1-24). More precisely, the magic numbers $|M_{1,12}|$ and $|M_{1,14}|$ equal 3 whereas, that $|M_{1,24}|$ is 2, which means that $(M_{1,12}/M_{1,24})^2 = (3)^2/(2)^2 = 2.25$. Thus the transmission coefficients associated with contact sites (1-12) and (1-14) should be (2.25) times higher than that associated with contact site (1-24).

The MRR is an exact formula for conductance ratios of a tight binding representation of the molecule in the weak-coupling limit, when the Fermi energy is located at the center of the HOMO-LUMO gap. Therefore, as expected the transmission coefficients ratios obtained from tight binding calculations in Figure 4.2 are similar to MRR predictions.

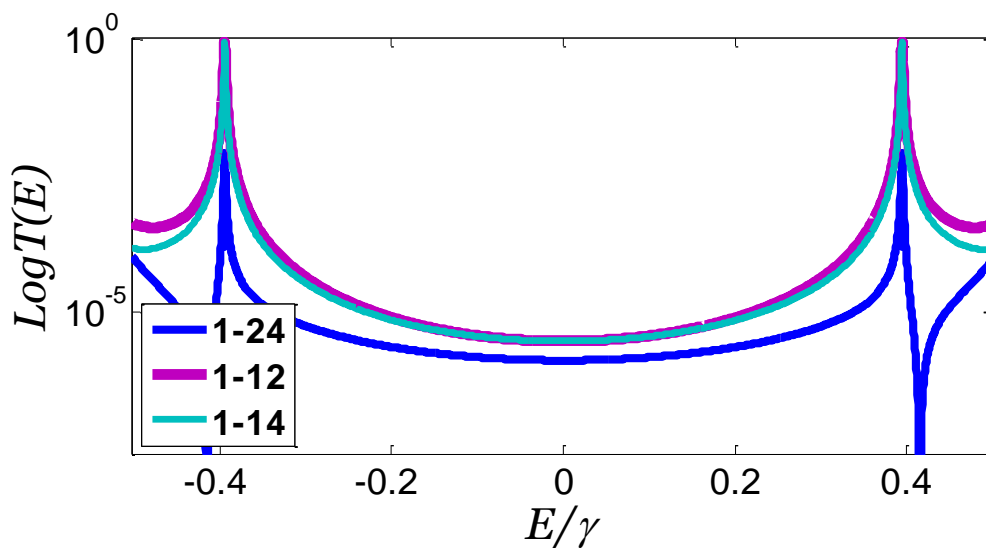


Figure 4.2: Transmission coefficients $T_{ij}(E)$ of the molecule obtained from tight binding calculations.

To verify the MRR prediction, theoretical calculations based on density functional theory (DFT) and non-equilibrium Green's functions NEGF have been done in order to obtain the transmission coefficients $T_{ij}(E)$ describing electrons passing through the core of the molecule from one electrode to the other. Figure 4.3 shows the tris(benzocyclobutadieno)triphenylene molecule placed between two identical compound electrodes where the compound electrodes are composed of linker groups comprising carbon-carbon triple bond (left panel) and carbon triple bond connected to pyridine anchor (right panel), which in turn are connected to the gold electrodes.

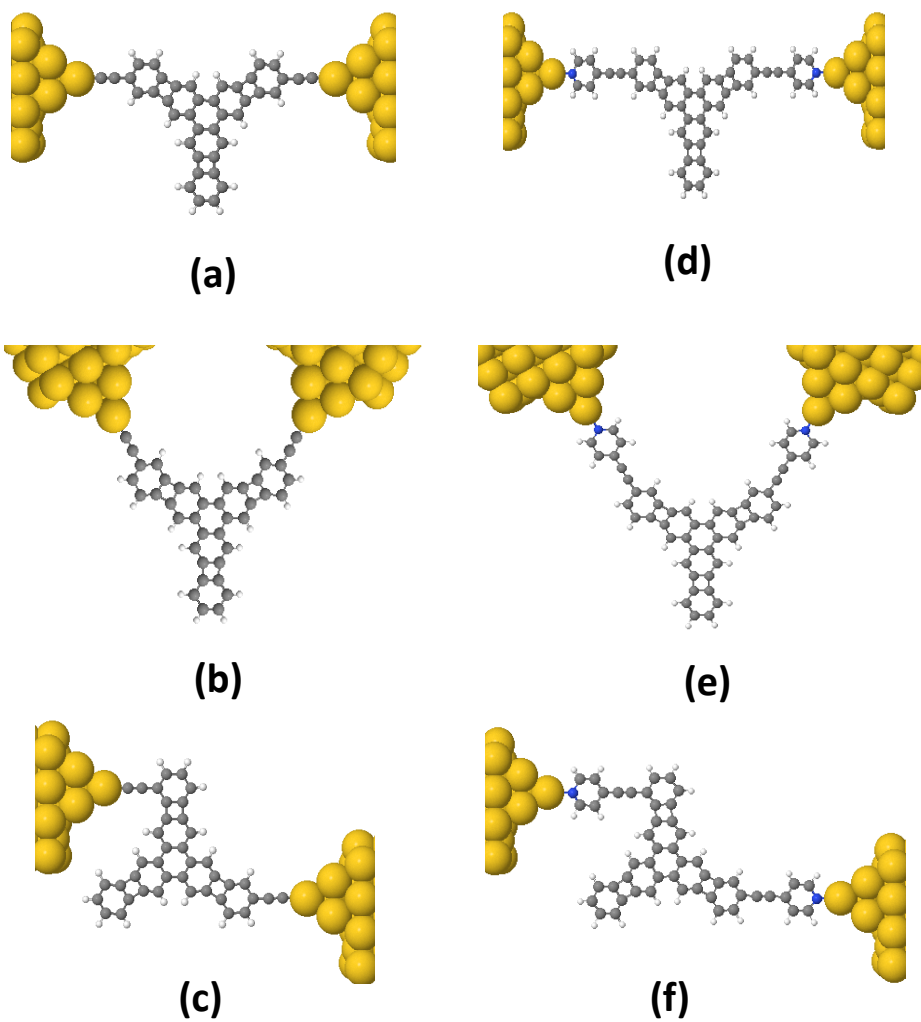


Figure 4.3:The tris(benzocyclobutadieno)triphenylene molecule connected to two gold electrodes via: (a-c) carbon-carbon triple bond linker and (d-f) pyridyl linker where, (a,d) , (b,e) and (c,f) correspond to (1-24) , (1-12) and (1-14) connectivities, respectively.

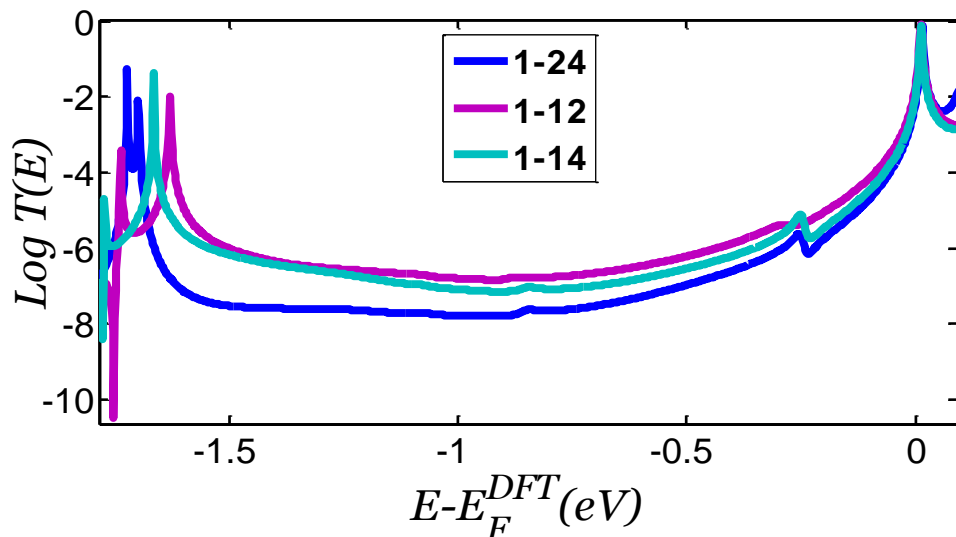


Figure 4.4 : DFT results for the transmission coefficients of tris(benzocyclobutadieno)-triphenylene using pyridyl anchoring groups.

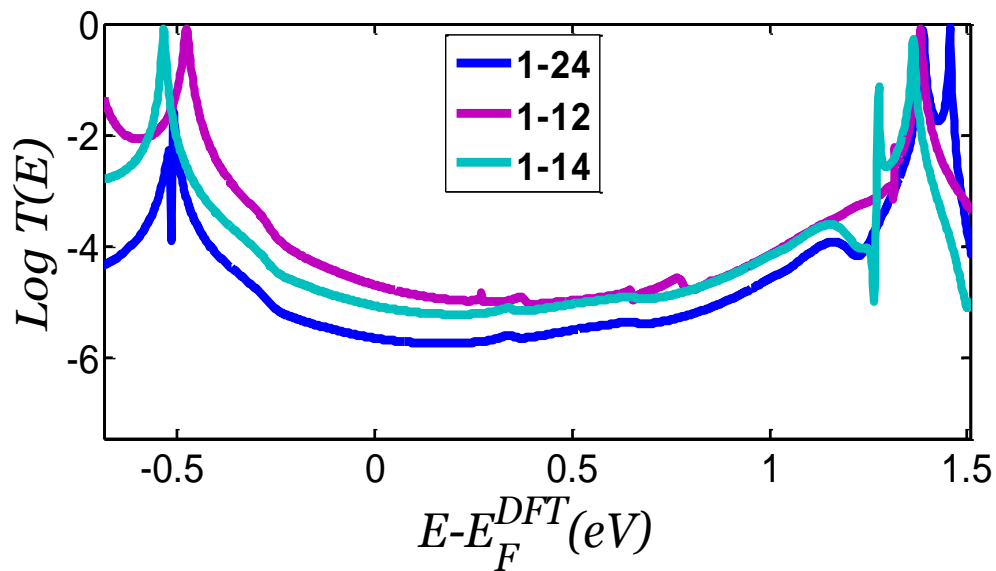


Figure 4.5: DFT results for the transmission coefficients of tris-(benzocyclobutadieno)triphenylene using carbon-carbon triple bond anchoring groups.

Figures 4.4 and 4.5 show the transmission coefficients of tris(benzocyclobutadieno)triphenylene as a function of the Fermi energy E_F of the electrodes for different anchoring groups, pyridyl and carbon-carbon triple bond, respectively. As predicted by the MRR, the transmission coefficients of tris(benzocyclobutadieno)-triphenylene with (1-12) (purple curve) and (1-14) (magenta curve) connectivities are quite similar over a range of energy near the mid gap and higher than the transmission coefficient of the (1-24) connectivity (blue curve). In details, Figure 4.4 shows that the calculated transmission coefficient related to contact sites (1-12) and (1-14) is (2.4) times higher than that with contact site (1-24) at $E = -0.26$ where, for Figure 4.5 the transmission coefficient ratio of (2.4) was achieved at some range of energy. However, whatever value is chosen within the HOMO-LUMO gap, the transmission coefficients trends in both figures are in good agreement with the MRR trend.

As mentioned previously, the tris(benzocyclobutadieno)triphenylene is composed of three biphenylene molecules linked to each other through a benzene ring. The biphenylene itself is an interesting molecule and in turn consist of two benzene rings connected by a cyclobutadiene ring. According to the Hückel's rules, the electronic structure with $4n$ π -electrons gives the

biphenylene an antiaromatic character [16, 17]. However, the relatively long distance between the two benzene rings weakens the bond of the cyclobutadiene ring leading biphenylene to intermediate behaviour between aromatic and antiaromatic molecule [18, 19], which explains why biphenylene is a stable molecule, but more reactive than benzene[20]. This intermediate aromatic and anti-aromatic behaviour and the high conductivity[21] makes the biphenylene a target of several experimental and theoretical studies[21, 22]. Moreover, the biphenylene molecule is an interesting new candidate as a building block for advanced 2D materials so-called biphenylene carbon (BPC), which is expected to play a major role as a novel organic material [23, 24].

The aim of this section is to apply the MRR to another antiaromatic molecule (biphenylene) to further confirm the validity of this rule for antiaromatic compounds and to compare the transport properties of the biphenylene molecule with that of the aromatic molecules, naphthalene and anthracene, with different connectivities. Let us start by creating M-tables for these molecules shown in Figure 4.6.

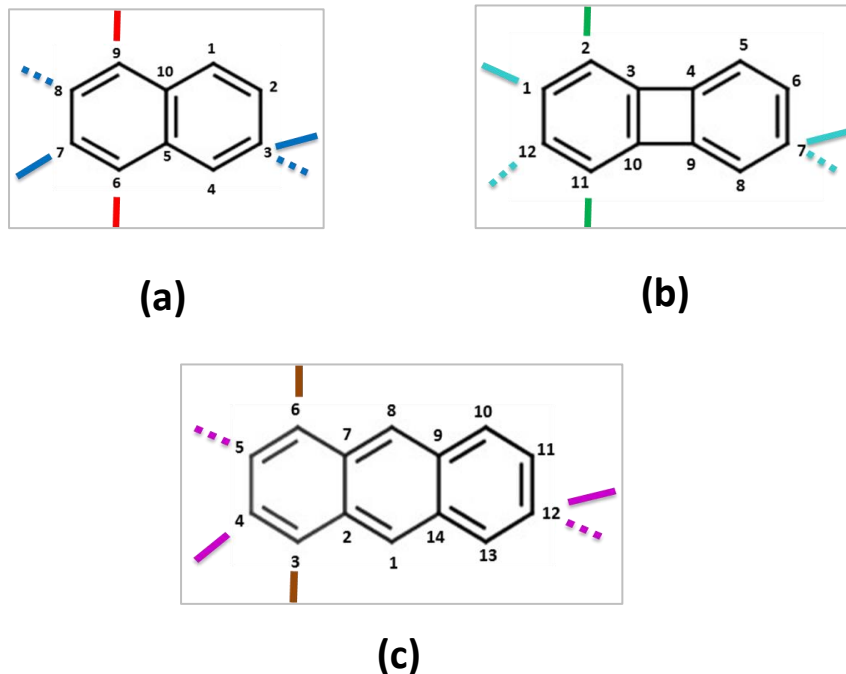


Figure 4.6: Molecular structures of: (a) naphthalene, (b) biphenylene and (c) anthracene associated with different connectivities.

Tables 4.2 (a-c), represent the M-tables of naphthalene, biphenylene and anthracene respectively. As mentioned earlier, the non-zero M_{ij} values in these tables correspond to odd to even (or vice versa) connectivities which result in constructive interference, whereas all odd to odd and even to even connectivities lead to $M_{ij} = 0$ (not shown here) and correspond to destructive interference.

(a)

M_{ij}	2	4	6	8	10
1	-2	2	-1	1	-1
3	-1	-2	1	-1	1
5	1	-1	-1	1	-1
7	-1	1	-2	-1	1
9	1	-1	2	-2	-1

(b)

M_{ij}	2	4	6	8	10	12
1	-1	-1	1	-1	2	-2
3	-2	1	-1	1	-2	2
5	1	-2	-1	1	1	-1
7	-1	2	-2	-1	-1	1
9	1	-2	2	-2	1	-1
11	1	1	-1	1	-2	-1

(c)

M_{ij}	2	4	6	8	10	12	14
1	-2	2	-2	4	-2	2	-2
3	-1	-3	3	-2	1	-1	1
5	1	-1	-3	2	-1	1	-1
7	-1	1	-1	-2	1	-1	1
9	1	-1	1	-2	-1	1	-1
11	-1	1	-1	2	-3	-1	1
13	1	-1	1	-2	3	-3	-1

Table 4.2: The M-tables of : (a) naphthalene, (b) biphenylene and (c) anthracene, respectively, correspond to odd to even connectivities (note that all odd to odd and even to even elements are zero).

Based on M-tables in Table 4.2, the transmission coefficients associated with contact sites (3-8), (7-12), and (12-5) of the naphthalene, biphenylene and anthracene, respectively, should be higher than that of the corresponding odd to odd and even to even connectivities ((3-7), (7-1), (12-4)). The tight

binding calculations in Figure 4.7 show very similar results for wide range of energy at the middle of the HOMO-LUMO gap. Furthermore, the transmission coefficients values of naphthalene (blue dotted curve) and biphenylene (magenta dotted curve) are equal and very close to the transmission coefficient value of anthracene (purple dotted curve) at the middle of HOMO-LUMO gap. In turn, these transmission coefficients are higher than those associated with odd to odd or even to even connectivities, (3-7) for naphthalene (blue solid curve), (7-1) for biphenylene (magenta solid curve) and (12-4) for anthracene (purple solid curve).

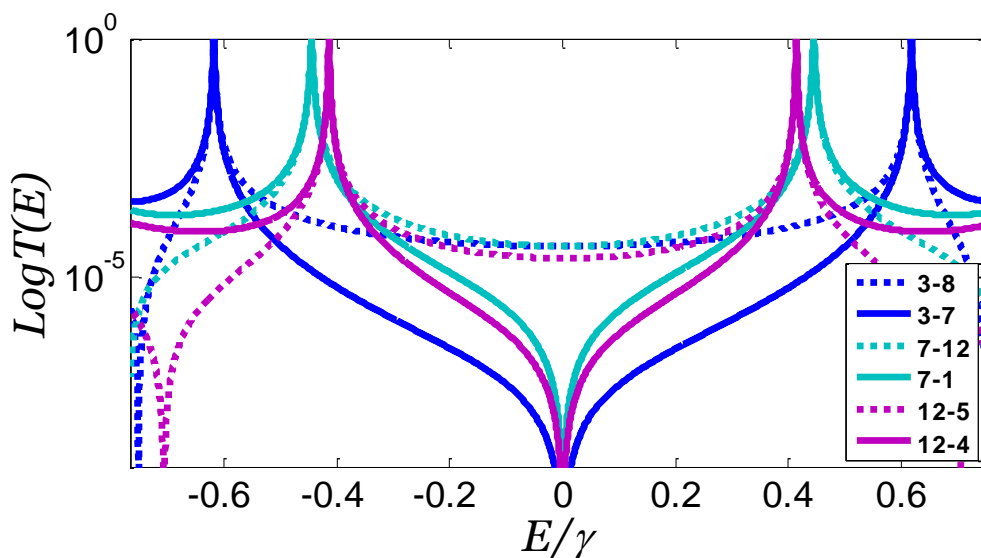


Figure 4.7: Tight binding representations of the transmission coefficients $T_{ij}(E)$ of the naphthalene (blue curves), biphenylene (magenta curves) and anthracene (purple curves), where solid lines correspond to even(odd) to even(odd) connectivities and dotted lines correspond to odd to even connectivities.

Having introduced the tight binding calculations, I will now show DFT calculations of the transmission coefficients $T_{ij}(E)$ describing electrons passing through the core of a molecule from one compound electrode to the other. Figure 4.8 shows the relaxed structure of the three molecules attached to “compound electrodes” comprising acetylene linkers attached via phenyl rings and a thiol anchor to gold electrodes.

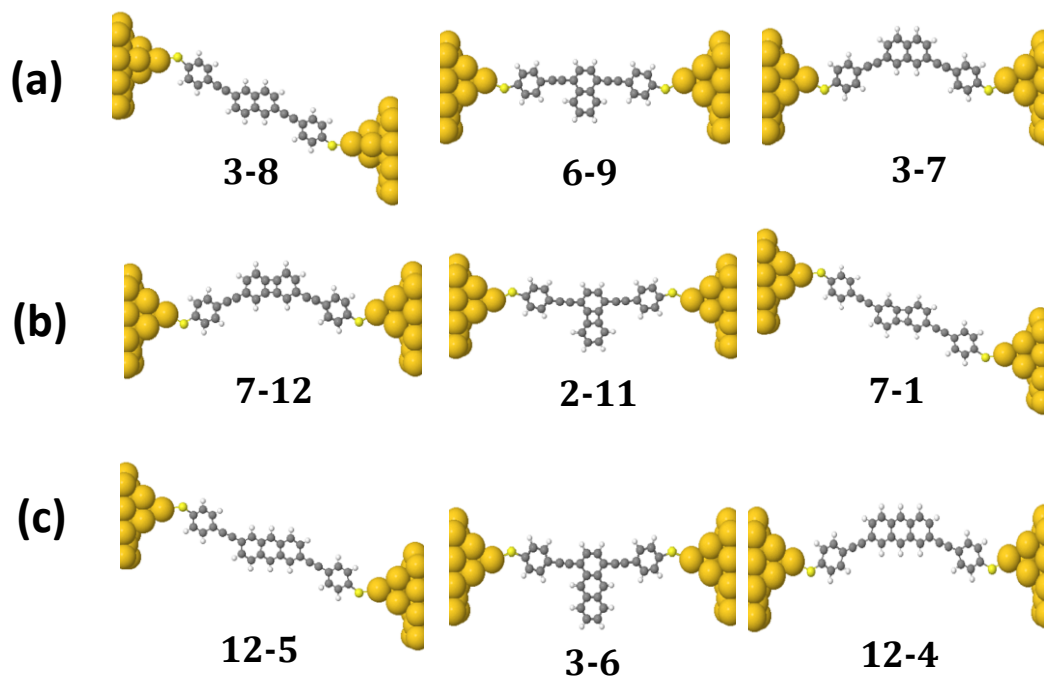


Figure 4.8: Relaxed structures with different connectivities of (a) naphthalene, (b) biphenylene and (c) anthracene.

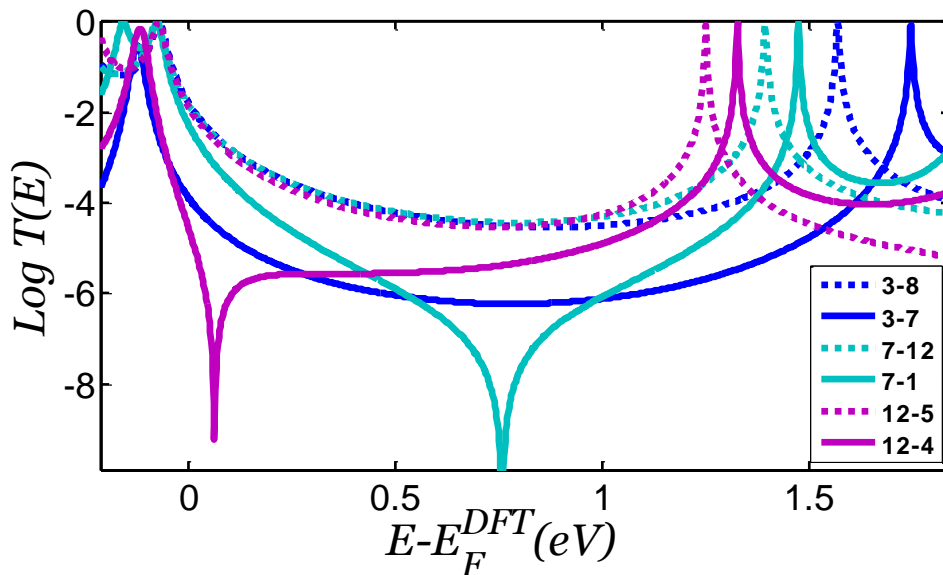


Figure 4.9: DFT results of the transmission coefficients $T_{ij}(E)$ of the naphthalene (blue curves), biphenylene (magenta curves) and anthracene (purple curves), where solid lines correspond to even(odd)-even(odd) connectivities and dotted lines correspond to odd to even connectivities.

Figure 4.9 shows the transmission coefficients of naphthalene, biphenylene and anthracene as a function of the Fermi energy E_F of the electrodes, obtained from a transport calculation using a combination of density functional theory DFT and non-equilibrium Green's functions. As shown in this figure, the transmission coefficient of naphthalene and biphenylene are similar and slightly higher than that of anthracene and also the transmission coefficients of odd to even (or vice versa) connectivities for the three

molecules (dotted curves) are higher than that of odd(even) to odd(even) connectivities (solid curves), which agrees with tight binding result.

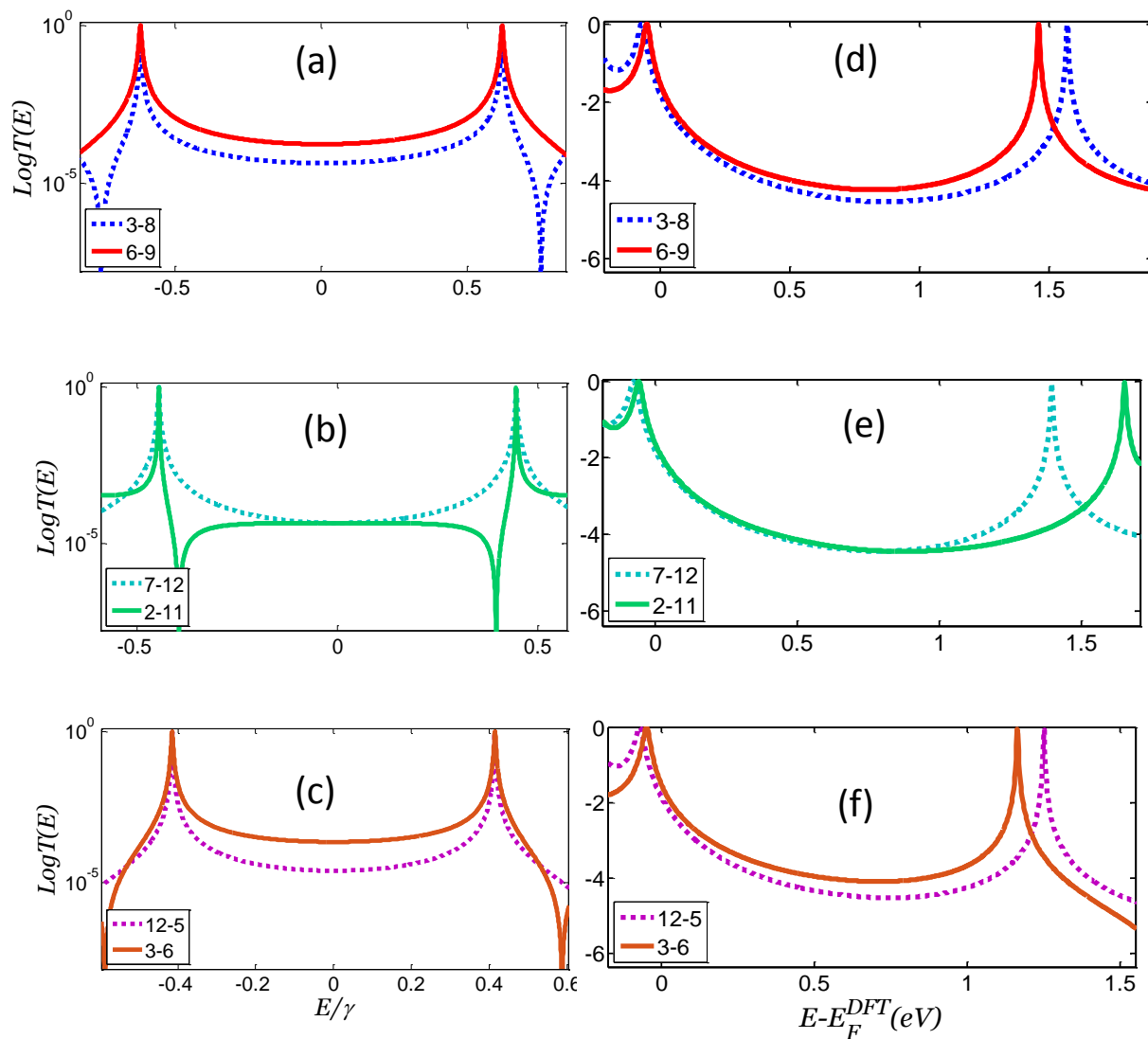


Figure 4.10: The transmission coefficients obtained: (a-c) using tight binding calculations and (d-f) DFT calculations for naphthalene (a,d), biphenylene (b,e) and anthracene (c,f) for two different odd to even connectivities.

Figure 4.10 compares the transmission coefficients for two different odd-even (or vice versa) connectivities through each molecule. Usually, one would expect to obtain a higher conductance for the shorter path through the molecule compared with the longer path. Surprisingly, this is not the case for biphenylene, where its M-table indicates that the transmission coefficients associated with the connectivities (7-12) (long path) and (2-11) (short path) are equal. For the other molecules, the M-tables predictions are as expected where the transmission coefficients related to the contact sites (6-9), (3-6) higher than those with contact sites (3-8), (12-5) for naphthalene, anthracene respectively.

Figure 4.10 shows the transmission coefficients of the three molecules, (a-c) obtained from the tight binding calculations and (d-f) obtained from DFT-NEGF calculations . As predicted surprisingly from MRR, Figure 4.10 (b,e) show that the transmission coefficients of the biphenylene with (7-12) (magenta curves) and (2-11) (green curves) connectivities are equal. On the other hand, Figure 4.10 (a,d) and (c,f) show that the transmission coefficients of the naphthalene and anthracene with (6-9) (red curves) and (3-6) (brown curves) are higher than the transmission coefficients associated with contact sites (3-8) (blue curves) and (12-5) (purple curves) respectively. The following table shows a comparison between MRR predictions and the

corresponding results obtained from DFT for the transmission coefficient ratios of two different odd to even connectivities for each molecule. Clearly, the results shown in this table demonstrate a good agreement between the MRR and DFT.

Molecule	Odd to Even connectivities	MRR	DFT Ratio
Naphthalene	(6-9), (3-8)	$\left(\frac{2}{-1}\right)^2 = 4$	4 at $E = 1.32 \text{ eV}$
Biphenylene	(7-12), (2,11)	$\left(\frac{1}{1}\right)^2 = 1$	1 over the range $0.09 < E < 0.89$
Anthracene	(3-6), (12-5)	$\left(\frac{3}{1}\right)^2 = 9$	9 at $E = 1.1 \text{ eV}$

4.3 Conclusion

It has been demonstrated that the MRR correctly predicts the conductance ratios of polycyclic aromatic hydrocarbons (PAH). In order to explore a new class of molecules, I have carried out a theoretical study based on tight binding and DFT calculations to examine the MRR for antiaromatic cores. I tested tris(benzocyclobutadieno)triphenylene and biphenylene molecules. For tris(benzocyclobutadieno)triphenylene I have calculated the transmission coefficients using two different anchoring groups: pyridyl and carbon-carbon

triple bond . The DFT results show that, whatever value is chosen within the HOMO-LUMO gap, the transmission coefficient trends for both anchors are in good agreement with the MRR. Furthermore, comparing the transmission coefficient of biphenylene with that of naphthalene and anthracene for different connectivities and also comparing the transmission coefficients for different connectivities through biphenylene using DFT yields good agreement with the MRR over a wide range of energy, which means that the MRR can be apply for polycyclic antiaromatic hydrocarbons (PAAH).

4.4 Calculations methods

DFT calculations: The optimized geometry and ground state Hamiltonian and overlap matrix elements of each structure was self-consistently obtained using the SIESTA [25] implementation of density functional theory (DFT). SIESTA employs norm-conserving pseudo-potentials to account for the core electrons and linear combinations of atomic orbitals to construct the valence states. The generalized gradient approximation (GGA) of the exchange and correlation functional is used with the Perdew-Burke-Ernzerhof parameterization (PBE) a double- ζ polarized (DZP) basis set, a real-space grid defined with an equivalent energy cut-off of 250 Ry. The geometry

optimization for each structure is performed to the forces smaller than 10 meV/Ang.

Transport calculations: The mean-field Hamiltonian obtained from the converged DFT calculation or a tight-binding Hamiltonian (using single orbital energy site per atom with Hückel parameterisation) was combined with implementation non-equilibrium Green's function method, GOLLUM [26], to calculate the phase-coherent, elastic scattering properties of the each system consisting of left gold (source) and right gold (drain) leads and the scattering region (molecule). The transmission coefficient $T(E)$ for electrons of energy E (passing from the source to the drain) is calculated via the relation: $T(E) = \text{Trace}(\Gamma_R(E)G^R(E)\Gamma_L(E)G^{R\dagger}(E))$. In this expression, $\Gamma_{L,R}(E) = i(\Sigma_{L,R}(E) - \Sigma_{L,R}^\dagger(E))$ describe the level broadening due to the coupling between left (L) and right (R) electrodes and the central scattering region, $\Sigma_{L,R}(E)$ are the retarded self-energies associated with this coupling and $G^R = (ES - H - \Sigma_L - \Sigma_R)^{-1}$ is the retarded Green's function, where H is the Hamiltonian and S is overlap matrix. Using obtained transmission coefficient $T(E)$, the conductance could be calculated by Landauer formula ($G = G_0 \int dE T(E)(-\partial f/\partial E)$) where $G_0 = 2e^2/h$ is conductance quantum.

References

- [1] F. Chen and N. J. Tao, "Electron Transport in Single Molecules: From Benzene to Graphene," *Accounts of Chemical Research*, vol. 42, pp. 429-438, 2009/03/17 2009.
- [2] W. Pisula, X. Feng, and K. Müllen, "Charge-Carrier Transporting Graphene-Type Molecules," *Chemistry of Materials*, vol. 23, pp. 554-567, 2011/02/08 2011.
- [3] R. L. Carroll and C. B. Gorman, "The Genesis of Molecular Electronics," *Angewandte Chemie International Edition*, vol. 41, pp. 4378-4400, 2002.
- [4] J. Cai, P. Ruffieux, R. Jaafar, M. Bieri, T. Braun, S. Blankenburg, *et al.*, "Atomically precise bottom-up fabrication of graphene nanoribbons," *Nature*, vol. 466, pp. 470-3, Jul 22 2010.
- [5] F. Feixas, E. Matito, M. Solà, and J. Poater, "Analysis of Hückel's $[4n + 2]$ Rule through Electronic Delocalization Measures," *The Journal of Physical Chemistry A*, vol. 112, pp. 13231-13238, 2008/12/18 2008.
- [6] J. Juselius and D. Sundholm, "Polycyclic antiaromatic hydrocarbons," *Phys Chem Chem Phys*, vol. 10, pp. 6630-4, Nov 28 2008.

- [7] S. Shetty, D. G. Kanhere, and S. Pal, "Metallo-Antiaromatic Al₄Na₄ and Al₄Na₃- Compounds: A Theoretical Investigation," *The Journal of Physical Chemistry A*, vol. 108, pp. 628-631, 2004/01/01 2004.
- [8] S. Fujii, S. Marqués-González, J.-Y. Shin, H. Shinokubo, T. Masuda, T. Nishino, *et al.*, "Highly-conducting molecular circuits based on antiaromaticity," vol. 8, p. 15984, 07/19/online 2017.
- [9] C. J. Lambert, "Basic concepts of quantum interference and electron transport in single-molecule electronics," *Chemical Society Reviews*, vol. 44, pp. 875-888, 2015.
- [10] N. Kepčija, Y.-Q. Zhang, M. Kleinschrodt, J. Björk, S. Klyatskaya, F. Klappenberger, *et al.*, "Steering On-Surface Self-Assembly of High-Quality Hydrocarbon Networks with Terminal Alkynes," *The Journal of Physical Chemistry C*, vol. 117, pp. 3987-3995, 2013/02/28 2013.
- [11] W. Changsheng, S. B. Andrei, R. B. Martin, J. A. Geoffrey, U. Barbara, G. Iain, *et al.*, "Electrical characterization of 7 nm long conjugated molecular wires: experimental and theoretical studies," *Nanotechnology*, vol. 18, p. 044005, 2007.
- [12] Y. Geng, S. Sangtarash, C. Huang, H. Sadeghi, Y. Fu, W. Hong, *et al.*, "Magic Ratios for Connectivity-Driven Electrical Conductance of

- Graphene-like Molecules," *Journal of the American Chemical Society*, vol. 137, pp. 4469–4476, 2015/03/17 2015.
- [13] S. Sangtarash, C. Huang, H. Sadeghi, G. Sorohhov, J. Hauser, T. Wandlowski, *et al.*, "Searching the Hearts of Graphene-like Molecules for Simplicity, Sensitivity, and Logic," *Journal of the American Chemical Society*, vol. 137, pp. 11425-11431, 2015/09/09 2015.
- [14] B. Iglesias, A. Cobas, D. Perez, E. Guitian, and K. P. Vollhardt, "Tris(benzocyclobutadieno)triphenylene and its lower biphenylene homologues by palladium-catalyzed cyclizations of 2,3-didehydrobiphenylene," *Org Lett*, vol. 6, pp. 3557-60, Sep 30 2004.
- [15] M. M. Haley, "Advances in Strain in Organic Chemistry, Volume 5 Edited by Brian Halton (Victoria UniversityWellington). JAI Press: Greenwich, CT. 1996. xi + 287 pp. \$97.50. ISBN 0-7623-0075-2," *Journal of the American Chemical Society*, vol. 118, pp. 11694-11694, 1996/01/01 1996.
- [16] R. Breslow, J. Brown, and J. J. Gajewski, "Antiaromaticity of cyclopropenyl anions," *Journal of the American Chemical Society*, vol. 89, pp. 4383-4390, 1967/08/01 1967.
- [17] R. Breslow, "Novel aromatic and antiaromatic systems," *Chem Rec*, vol. 14, pp. 1174-82, Dec 2014.

- [18] J. Lüder, M. de Simone, R. Totani, M. Coreno, C. Grazioli, B. Sanyal, *et al.*, "The electronic characterization of biphenylene—Experimental and theoretical insights from core and valence level spectroscopy," *The Journal of Chemical Physics*, vol. 142, p. 074305, 2015/02/21 2015.
- [19] H. E. Baumgarten, "Mechanism and Theory in Organic Chemistry, Third Edition (Lowry, Thomas H.; Richardson, Kathleen Schuller)," *Journal of Chemical Education*, vol. 66, p. A131, 1989/04/01 1989.
- [20] T. W. Bell, "Book Review: Fascinating Molecules in Organic Chemistry. By F. Vögtle," *Angewandte Chemie International Edition in English*, vol. 32, pp. 306-307, 1993.
- [21] A. I. S. Holm, H. A. B. Johansson, H. Cederquist, and H. Zettergren, "Dissociation and multiple ionization energies for five polycyclic aromatic hydrocarbon molecules," *The Journal of Chemical Physics*, vol. 134, p. 044301, 2011/01/28 2011.
- [22] R. Totani, C. Grazioli, T. Zhang, I. Bidermane, J. Lüder, M. de Simone, *et al.*, "Electronic structure investigation of biphenylene films," *The Journal of Chemical Physics*, vol. 146, p. 054705, 2017/02/07 2017.
- [23] G. Brunetto, P. A. S. Autreto, L. D. Machado, B. I. Santos, R. P. B. dos Santos, and D. S. Galvão, "Nonzero Gap Two-Dimensional

- Carbon Allotrope from Porous Graphene," *The Journal of Physical Chemistry C*, vol. 116, pp. 12810-12813, 2012/06/14 2012.
- [24] J. Lüder, C. Puglia, H. Ottosson, O. Eriksson, B. Sanyal, and B. Brena, "Many-body effects and excitonic features in 2D biphenylene carbon," *The Journal of Chemical Physics*, vol. 144, p. 024702, 2016/01/14 2016.
- [25] M. S. José, A. Emilio, D. G. Julian, G. Alberto, J. Javier, O. Pablo, *et al.*, "The SIESTA method for ab initio order- N materials simulation," *Journal of Physics: Condensed Matter*, vol. 14, p. 2745, 2002.
- [26] J. Ferrer, C. J. Lambert, V. M. García-Suárez, D. Z. Manrique, D. Visontai, L. Oroszlany, *et al.*, "GOLLUM: a next-generation simulation tool for electron, thermal and spin transport," *New Journal of Physics*, vol. 16, p. 093029, 2014.

Chapter 5

Theoretical Study of Conductance Ratios for Different Connectivities in C_{60} Molecule.

5.1 Introduction:

For centuries, carbon has been known to exist in two very different natural crystalline forms, gray conductive graphite and transparent insulating diamond[1]. In 1986, the new form of carbon, Buckminsterfullerene (C_{60}), was discovered[2]. Besides diamond, graphite, and fullerene, quasi-one-dimensional nanotubes are another form of carbon, which was discovered shortly afterwards[3]. These new materials show properties that are completely different from the earlier known forms, diamond and graphite. Buckyballs are composed of carbon atoms linked to three other carbon atoms bonded in a spherical shape[4]. (C_{60}) and other fullerenes are outstanding molecules due to their chemical, mechanical and optical properties and have found several applications in science and technology. The first useful property comes from

their large capacity of the internal space which affords the possibility of placing atoms of different elements inside the molecular cage of the carbon atoms[5]. Fullerenes are also known as strong electron acceptors which help in the fabrication of donor-acceptor nano-junctions [6]. Interestingly, fullerenes share the softness of graphite, however, when they are compressed to less than 70% of their volumes, they become harder than diamond, in particular, (C_{60}) displays unusual electrical properties under simple compression. Moreover, the spherical structure (high symmetry) and the carbon to carbon bonds of (C_{60}) make it incredibly stable [7]. Therefore, (C_{60}) is considered as an ideal candidate for molecular-based devices.

Since fullerenes were discovered, the aromaticity related to these molecules has been the focus of debate. Huckel's rule states that cyclic planar conjugated compounds with $(4n + 2)\pi$ electrons such as benzene [8] are aromatic. Consequently, the fullerenes including (C_{60}) are classified as non-aromatic molecules because they are not planar and fail to satisfy Huckel's rule. Moreover, (C_{60}) does not obey Hirsch's rule [9] for spherical aromatic components. where the spherical aromatic molecule must possess $2(N + 1)^2\pi$ electrons. As a result, (C_{60}) is a spherically non-aromatic molecule[10, 11].

5.2 Magic numbers for C_{60}

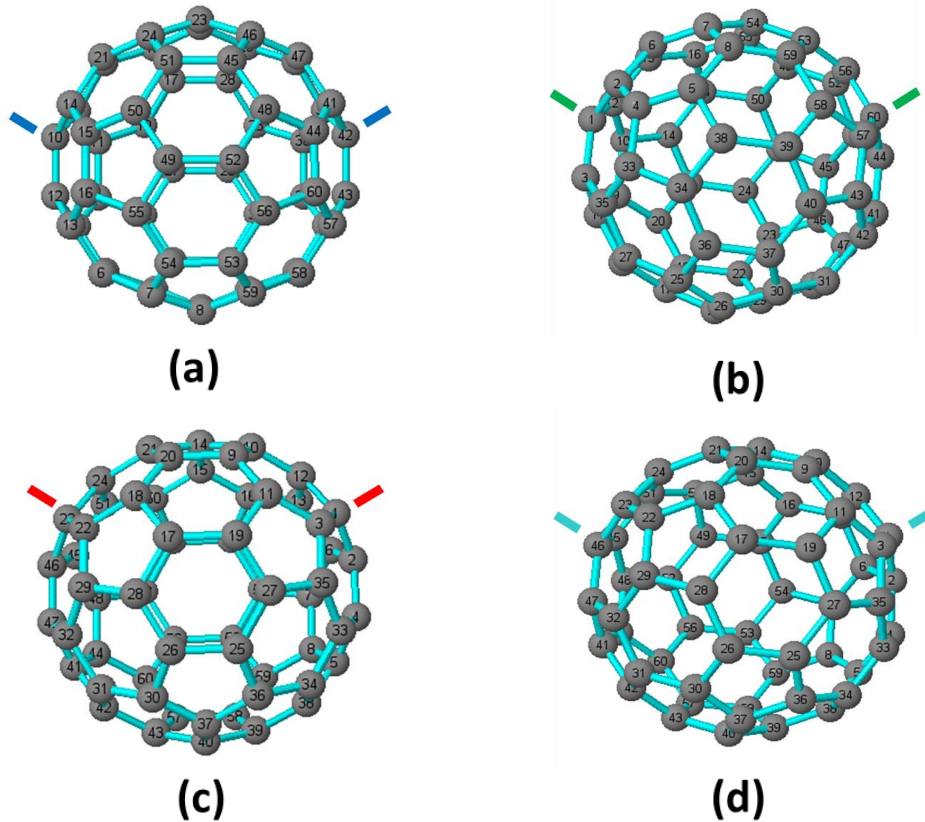


Figure 5.1: Molecular structure of (C_{60}) with different connectivities: (a), (b), (c) and (d) correspond (10-42), (1-60), (1-23) and (1-46) connectivity, respectively

In the molecular electronics community, quantum interference (QI) plays a vital role in determining the electrical conductance of single molecules. Within the phase-coherent regime, electron transport through a single molecule junction is described by transmission probability $T(E)$, and then the electrical conductance can be obtained. In earlier chapters, I showed that the MRR can be

used to predict the electrical conductance ratios arising from constructive QI in aromatic and antiaromatic molecules [12,13]. The main goal of the present work is to examine the validity of the MRR for the buckyball C_{60} which is known as non-aromatic molecule, shown in Figure 5.1. This shows that C_{60} is a spherical network of three-fold vertices, which due to its spherical topology, must contain both 6-membered and 5-membered rings [14].

Some examples of connectivities	Magic numbers $M_{ii'}$
1-9 , 24-18	43
1-10 , 2-7	1
1-14 , 9-13	-20
1-15 , 10-42	9
1-16 , 11-14	16
1-23 , 7-24	19
2-15 , 10-22	-14
2-22 , 5-20	-15
3-11 , 10-14	-23
4-2 , 12-10	-58
4-9 , 5-16	-26
5-10 , 8-25	8
5-24 , 8-18	-4
6-19 , 10-29	-5
6-21 , 6-18	7
7-10 , 11-15	-13
8-11 , 8-17	-3
8-22 , 13-31	3
1-46 , 1-60	0
8-18 , 8-29	-4

Table 5.1: Some examples of connectivities and their magic numbers are extracted from the M-table of C_{60} .

Using MRR requires creating an M-table composed of magic numbers M_{ij} related to the molecule of interest. For C_{60} , the M-table is 60x60 table which is too large to be displayed here. Instead I introduce a smaller table, which contains all possible distinct connections which could differ by symmetry, as shown in Table 5.1.

This table shows all magic numbers taken from the M-table of (C_{60}). To examine the possibility of applying the MRR to (C_{60}), I choose the following connectivities: (10-42), (1-60), (1-23) and (1-46) from table 5.1. According to the MRR, the transmission coefficient of (C_{60}) associated with connectivity (1-23) should be higher than the transmission coefficient associated with connectivity (10-42) and these two in turn should be higher than the equally valued transmission coefficients related to contact sites (1-60) and (1-46). In detail, the magic integer numbers of connectivities (1-23) and (10-42) are $M_{1,23} = 19$ and $M_{10,42} = 9$, respectively and the ratio between them is $(M_{1,23}/M_{10,42})^2 = (19)^2/(9)^2 = 4.45$ which means that the transmission coefficient of (C_{60}) corresponding to connectivity (1-23) should be around 4 times higher than that associated with connectivity (10-42). These predictions are illustrated using tight binding model in Figure 5.2,

for which the MRR is an exact formula for transmission coefficient ratios in the weak-coupling limit, when the Fermi energy is located at the center of the HOMO-LUMO gap.

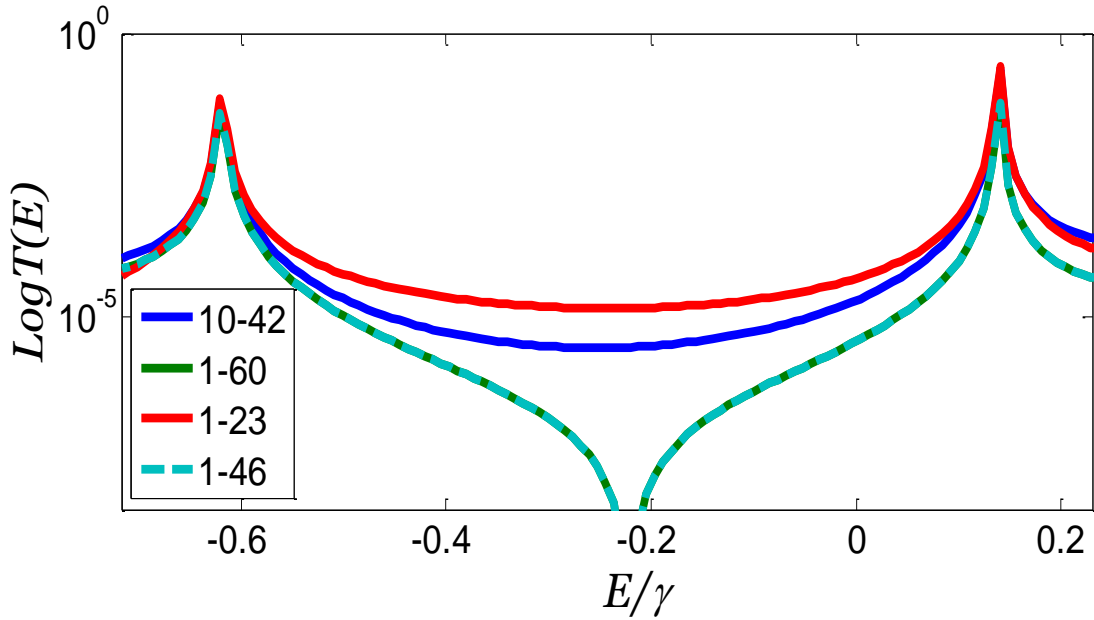


Figure 5.2: Tight binding representations of the transmission coefficients $T_{ij}(E)$ of (C_{60}) for different connectivities.

Figure 5.2 shows that the tight binding transmission coefficients follow the same trend of MRR over wide range of energies near the mid-gap, in which the transmission coefficient associated with contact site (1-23) (red curve) is higher than that with contact site (10-42) (blue curve) and for the other connectivities

(1-60) and (1-46) the transmission coefficients exhibit an antiresonance due to destructive interference.

To verify the MRR prediction, the transmission coefficients of C_{60} for the selected connectivities were calculated using DFT. In order to construct, firstly, the junction geometries, the (C_{60}) molecule was terminated by carbon-carbon triple bond anchoring groups [15] with respect to the four different connectivities and then the resulting compounds were relaxed using the SIESTA implementation of density functional theory (DFT) [16]. To the best of my knowledge, this is the first theoretical study of (C_{60}) transmission coefficients using carbon-carbon triple bond linkers for different connectivities. The second step was to place each relaxed compound between two identical gold electrodes. These structures were again geometrically relaxed with SIESTA to obtain optimal junction geometries as shown in Figure 5.3. Then the transmission coefficients $T(E)$ of electrons with energy E passing from one electrode to another through molecules were calculated using the GOLLUM transport code [17] (see methods).

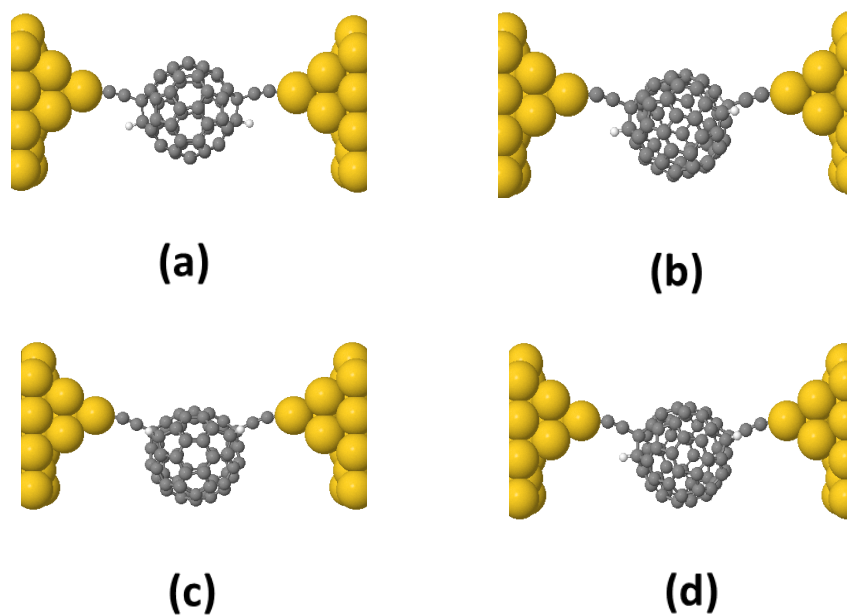


Figure 5.3: The C_{60} molecule connected to two gold electrodes through different connectivities via carbon-carbon triple bond linkers: (a), (b), (c) and (d) correspond (10-42), (1-60), (1-23) and (1-46) connectivity, respectively

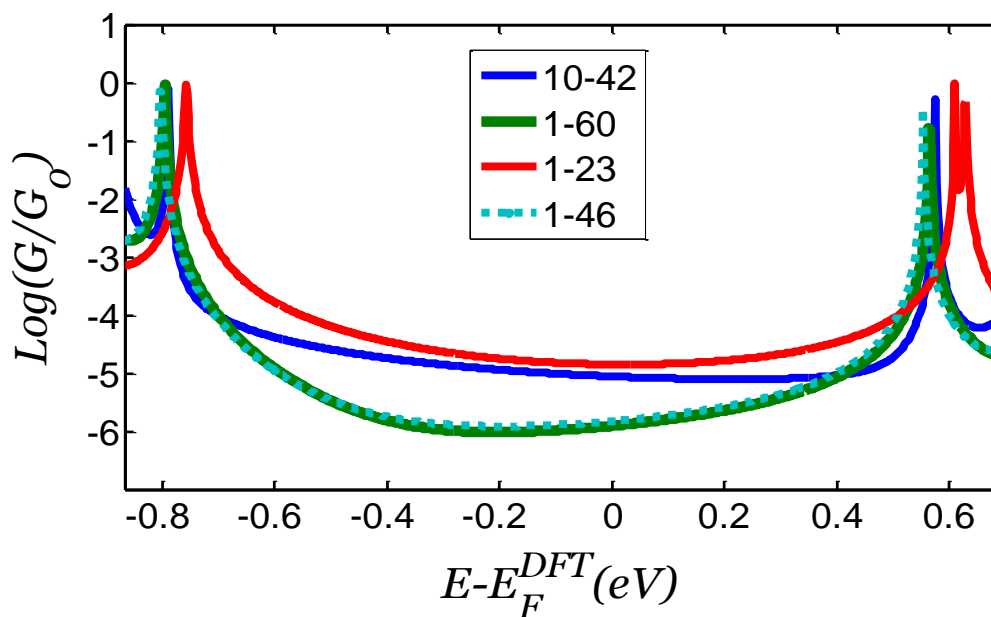


Figure 5.4: DFT results for the transmission coefficients of (C_{60}), where the blue, green, red and magenta curves correspond (10-42), (1-60), (1-23) and (1-46), respectively.

Although the four geometries in Figure 5.3 seem quite similar, they possess four different connectivities. The transmission coefficients curves of (C_{60}) compounds with respect to the selected connectivities resulting from DFT calculations are shown in Figure 5.4. This figure displays the same trend which is predicted using the MRR, where the transmission coefficient of connectivity (1-23) (red curve) is higher than that of connectivity (10-42) (blue curve) and in turn is higher than the transmission coefficient associated with (1-60) (green curve) and (1-46) (magenta curve) connectivities, where the last two are equal. For the ratios, I found an excellent agreement with DFT at $E = -0.61 \text{ eV}$, where the conductances ratio for (1-23) and (10-42) connectivities is (4.23) which is agreed with MRR prediction. However, whatever value is chosen within the HOMO-LUMO gap, the transmission coefficients trend is in good agreement with the MRR.

5.3 Conclusion

I have presented a theoretical study of the transmission coefficients of single molecule junction based on C_{60} molecules within four different connectivities. I connected the C_{60} to the electrodes via carbon-carbon triple bond anchoring groups. The transmission coefficients results of (C_{60}) obtained from DFT and tight binding calculations are in good agreement with the MRR predictions

which reflect the validity of the MRR in predicting the conductance ratios of fullerenes

5.4 Calculations methods

DFT calculations: The optimized geometry and ground state Hamiltonian and overlap matrix elements of each structure was self-consistently obtained using the SIESTA [15] implementation of density functional theory (DFT). SIESTA employs norm-conserving pseudo-potentials to account for the core electrons and linear combinations of atomic orbitals to construct the valence states. The generalized gradient approximation (GGA) of the exchange and correlation functional is used with the Perdew-Burke-Ernzerhof parameterization (PBE) a double- ζ polarized (DZP) basis set, a real-space grid defined with an equivalent energy cut-off of 250 Ry. The geometry optimization for each structure is performed to the forces smaller than 10 meV/Ang.

Transport calculations: The mean-field Hamiltonian obtained from the converged DFT calculation or a tight-binding Hamiltonian (using single orbital energy site per atom with Hückel parameterisation) was combined with implementation non-equilibrium Green's function method, GOLLUM [16], to calculate the phase-coherent, elastic scattering properties of the each system

consisting of left gold (source) and right gold (drain) leads and the scattering region (molecule). The transmission coefficient $T(E)$ for electrons of energy E (passing from the source to the drain) is calculated via the relation : $T(E) = \text{Trace}(\Gamma_R(E)G^R(E)\Gamma_L(E)G^{R\dagger}(E))$. In this expression, $\Gamma_{L,R}(E) = i(\Sigma_{L,R}(E) - \Sigma_{L,R}^\dagger(E))$ describe the level broadening due to the coupling between left (L) and right (R) electrodes and the central scattering region, $\Sigma_{L,R}(E)$ are the retarded self-energies associated with this coupling and $G^R = (ES - H - \Sigma_L - \Sigma_R)^{-1}$ is the retarded Green's function, where H is the Hamiltonian and S is overlap matrix. Using obtained transmission coefficient $T(E)$, the conductance could be calculated by Landauer formula ($G = G_0 \int dE T(E)(-\partial f/\partial E)$) where $G_0 = 2e^2/h$ is conductance quantum.

References

1. Kiguchi, M. and K. Murakoshi, *Conductance of Single C60 Molecule Bridging Metal Electrodes*. The Journal of Physical Chemistry C, 2008. **112**(22): p. 8140-8143.
2. Kroto, H., *C60 and carbon: a postbuckminsterfullerene perspective*. International Journal of Mass Spectrometry, 2000. **200**(1): p. 253-260.
3. Saifuddin, N., A.Z. Raziah, and A.R. Junizah, *Carbon Nanotubes: A Review on Structure and Their Interaction with Proteins*. Journal of Chemistry, 2013. **2013**: p. 18.
4. Jamal-Omidi, M., M. ShayanMehr, and R. Rafiee, *A Study on Equivalent Spherical Structure of Buckyball-C 60 Based on Continuum Shell Model*. Latin American Journal of Solids and Structures, 2016. **13**: p. 1016-1029.
5. Kuc, A., et al., *Hydrogen Sieving and Storage in Fullerene Intercalated Graphite*. Nano Letters, 2007. **7**(1): p. 1-5.
6. Guerin, D., et al., *Synthesis and electrical properties of fullerene-based molecular junctions on silicon substrate*. Journal of Materials Chemistry, 2010. **20**(13): p. 2680-2690.

7. Georgakilas, V., et al., *Broad Family of Carbon Nanoallotropes: Classification, Chemistry, and Applications of Fullerenes, Carbon Dots, Nanotubes, Graphene, Nanodiamonds, and Combined Superstructures*. Chemical Reviews, 2015. **115**(11): p. 4744-4822.
8. Feixas, F., et al., *Analysis of Hückel's $[4n + 2]$ Rule through Electronic Delocalization Measures*. The Journal of Physical Chemistry A, 2008. **112**(50): p. 13231-13238.
9. Hirsch, A., Z. Chen, and H. Jiao, *Spherical Aromaticity in I_h Symmetrical Fullerenes: The $2(N+1)2$ Rule*. Angewandte Chemie International Edition, 2000. **39**(21): p. 3915-3917.
10. Johansson, M.P., J. Jusélius, and D. Sundholm, *Sphere Currents of Buckminsterfullerene*. Angewandte Chemie International Edition, 2005. **44**(12): p. 1843-1846.
11. Munoz-Castro, A., *The shielding cone in spherical aromatic structures: insights from models for spherical $2(N + 1)2$ aromatic fullerenes*. Physical Chemistry Chemical Physics, 2017. **19**(20): p. 12633-12636.
12. Geng, Y., et al., *Magic Ratios for Connectivity-Driven Electrical Conductance of Graphene-like Molecules*. Journal of the American Chemical Society, 2015. **137**(13): p. 4469-4476.

13. S. Sangtarash, C. Huang, H. Sadeghi, G. Sorohhov, J. Hauser, T. Wandlowski, *et al.*, "Searching the Hearts of Graphene-like Molecules for Simplicity, Sensitivity, and Logic," *Journal of the American Chemical Society*, vol. 137, pp. 11425-11431, 2015/09/09 2015.
14. CJ Lambert, DL Weaire, *Theory of the arrangement of cells in a network*, *Metallography* 14 (4), 307-318 1981.
15. Bucci, N. and T.J.J. Müller, *Synthesis and electronic properties of (oligo)phenothiazine-ethynyl-hydro-C60 dyads*. *Tetrahedron Letters*, 2006. **47**(47): p. 8329-8332.
16. José, M.S., et al., *The SIESTA method for ab initio order- N materials simulation*. *Journal of Physics: Condensed Matter*, 2002. **14**(11): p. 2745.
17. Ferrer, J., et al., *GOLLUM: a next-generation simulation tool for electron, thermal and spin transport*. *New Journal of Physics*, 2014. **16**(9): p. 093029.

Chapter 6

Conclusions

My focus in this thesis was on single molecule transport properties of various molecules including building blocks such as furan, pyrrole, thiophene, cyclopentadiene, tris-(benzocyclobutadieno)triphenylene, biphenylene and C₆₀ e. In chapter 3, the main aim was to investigate the effect of molecular symmetry and quantum interference on the charge transport through single molecule junctions with five-membered core ring. I found that for the symmetric series **1-4**, the pyridyl anchors dominate the conductance and there is no statistically significant variation with core unit. In contrast, the conductances of the asymmetric series **5-8** are significantly lower than those of the symmetric series, reflecting the presence of destructive quantum interference. These theoretical calculations are in good agreement with the experimental findings. More importantly, the control of molecular asymmetry via the heteroatoms allows the tuning of destructive quantum interference in the charge transport through single-molecule junctions. I carried out further theoretical calculations using thiol linkers instead of pyridyl linkers, where using thiol anchoring groups gives **9-16** compounds. Clearly, to compare the results obtained using these two different anchors depends upon the position

of the Fermi energy. However, in general, I found that the DFT results of **9-12** compounds are similar to those of **1-4** compounds over a small energy range confirming the impact of the anchoring groups on the charge transport through the molecule. In contrast, the results of **13-16** compounds show evidence of destructive interference. I also calculated the binding energies of compounds **1-8** and **9-16** and the results indicate that the binding energy values are quite similar for both the symmetric **1-4** and asymmetric **5-8** compounds; the binding energies of the symmetric series are slightly higher than those of the asymmetric series but there is no strong effect of the molecular symmetry on the binding energies of **1-8** compounds.

In chapter 4, I introduced a theoretical study based on tight binding and DFT calculations to examine the MRR for antiaromatic cores. In particular I investigated tris(benzocyclobutadieno)triphenylene and biphenylene molecules. For tris-(benzocyclobutadieno)triphenylene, I calculated the transmission coefficients using two different anchoring groups: pyridyls and carbon-carbon triple bonds. The DFT results show that at any energy value chosen within the HOMO-LUMO gap, the transmission coefficients trends for both anchors are in good agreement with the MRR predictions. Furthermore, comparing the transmission coefficient of biphenylene with that of naphthalene and anthracene for different connectivities and also

comparing the transmission coefficients for different connectivities through biphenylene itself using DFT reveals good agreement with the M-table over a wide range of energies, which means that the MRR can be applied to polycyclic antiaromatic hydrocarbons (PAAH).

In chapter 5, I presented a theoretical study of the transmission coefficients of single molecule junctions based on C_{60} with different connectivities. I have connected C_{60} to the electrodes via carbon-carbon triple bond anchoring groups. The transmission coefficients results for C_{60} obtained from DFT and tight binding calculations are in good agreement with the MRR predictions, which reflects the validity of the MRR in predicting the conductance ratios of fullerenes.